THE JOURNAL OF BIOLOGICAL CHEMISTRY VOL. 288, NO. 30, pp. 22080–22095, July 26, 2013
Published in the U.S.A.

A Model of the Membrane-bound Cytochrome b_5-Cytochrome P450 Complex from NMR and Mutagenesis Data*[S]

Received for publication, December 24, 2012, and in revised form, May 14, 2013 Published, JBC Papers in Press, May 24, 2013, DOI 10.1074/jbc.M112.448225

Shivani Ahuja[‡], Nicole Jahr[‡], Sang-Choul Im[§], Subramanian Vivekanandan[‡], Nataliya Popovych[‡], Stéphanie V. Le Clair[‡], Rui Huang[‡], Ronald Soong[‡], Jiadi Xu[‡], Kazutoshi Yamamoto[‡], Ravi P. Nanga[‡], Angela Bridges[§1], Lucy Waskell[§], and Ayyalusamy Ramamoorthy[‡2]

From the [‡]Department of Chemistry and Biophysics, University of Michigan, Ann Arbor, Michigan 48109-1055 and the [§]Department of Anesthesiology, University of Michigan, and Veterans Affairs Medical Center, Ann Arbor, Michigan 48105

Background: $cytb_5$ modulates catalysis performed by cytsP450, *in vivo* and *in vitro*.
Results: The structure of full-length $cytb_5$ was solved by NMR, and the cytP450-binding site on $cytb_5$ was identified by mutagenesis and NMR.
Conclusion: A model of the $cytb_5$-cytP450 complex is presented. Addition of a substrate strengthens the $cytb_5$-cytP450 interaction.
Significance: The $cytb_5$-cytP450 complex structure will help unravel the mechanism by which $cytb_5$ regulates catalysis by cytP450.

Microsomal cytochrome b_5 ($cytb_5$) is a membrane-bound protein that modulates the catalytic activity of its redox partner, cytochrome P4502B4 (cytP450). Here, we report the first structure of full-length rabbit ferric microsomal $cytb_5$ (16 kDa), incorporated in two different membrane mimetics (detergent micelles and lipid bicelles). Differential line broadening of the $cytb_5$ NMR resonances and site-directed mutagenesis data were used to characterize the $cytb_5$ interaction epitope recognized by ferric microsomal cytP450 (56 kDa). Subsequently, a data-driven docking algorithm, HADDOCK (high ambiguity driven biomolecular docking), was used to generate the structure of the complex between cytP4502B4 and $cytb_5$ using experimentally derived restraints from NMR, mutagenesis, and the double mutant cycle data obtained on the full-length proteins. Our docking and experimental results point to the formation of a dynamic electron transfer complex between the acidic convex surface of $cytb_5$ and the concave basic proximal surface of cytP4502B4. The majority of the binding energy for the complex is provided by interactions between residues on the C-helix and β-bulge of cytP450 and residues at the end of helix α4 of $cytb_5$. The structure of the complex allows us to propose an interprotein electron transfer pathway involving the highly conserved Arg-125 on cytP450 serving as a salt bridge between the heme propionates of cytP450 and $cytb_5$. We have also shown that the addition of a substrate to cytP450 likely strengthens the $cytb_5$-cytP450 interaction. This study paves the way to obtaining valuable structural, functional, and dynamic information on membrane-bound complexes.

Cytochromes P450 (cytsP450)[3] are a ubiquitous superfamily of mixed-function oxygenases, which are found in all kingdoms of life but are especially abundant in eukaryotes. Humans possess 57 different membrane-bound cytsP450 (1). They are found in all tissues of the body and are responsible for influencing a dazzling array of biochemical and physiological processes, including embryonic development, blood coagulation, and the metabolism of carcinogens, environmental toxins, over 50% of drugs in use, vitamin D, and other exogenous and endogenous compounds (2, 3). Selected human cytsP450 (cytP45017A1 and cytP45019A1) are targets for the treatment of prostate and breast cancer, respectively (4, 5).

CytP450 catalyzes the insertion of one atom of "activated" molecular oxygen into the substrate, using two electrons from NAD(P)H and two protons from water. Electrons destined for cytP450 are first delivered to its redox partners, cytP450-reductase (CPR) and $cytb_5$, which then transfer the electrons to cytP450 (6). CPR is capable of transferring both electrons to cytP450; however, $cytb_5$ is capable of donating only the second

* This work was supported, in whole or in part, by National Institutes of Health Grants GM084018 and GM095640 (to A. R.) and GM094209 and GM035533 (to L. W.). This work was also supported by a Veterans Affairs merit grant (to L. W.).

[S] This article contains supplemental Figs. S1–S6 and Table S1.

The atomic coordinates and structure factors (code 2M33) have been deposited in the Protein Data Bank (http://wwpdb.org/).

The chemical shift assignments have been deposited in the Biological Magnetic Resonance Bank under accession number 18919.

[1] Present address: GlaxoSmithKline, Medicines Research Centre, Gunnels Wood Rd., Stevenage, Hertfordshire SG1 2NY, United Kingdom.

[2] To whom correspondence should be addressed: Dept. of Chemistry and Biophysics, University of Michigan, Ann Arbor, MI 48109-1055. Tel.: 734-647-6572; Fax: 734-764-3323; E-mail: ramamoor@umich.edu.

[3] The abbreviations used are: cytsP450, cytochromes P450; 1-CPI, 1-(4-chlorophenyl) imidazole; two-dimensional HSQC, two-dimensional heteronuclear single quantum coherence; BHT, 3,5-di-*tert*-butyl-4-hydroxytoluene; $cytb_5$, cytochrome b_5; cytP450, cytochrome P450; CPR, cytochrome P450 reductase; DHPC, 1,2-dihexanoyl-*sn*-glycero-3-phosphocholine; DLPC, 1,2-dilauroyl-*sn*-glycero-3-phosphocholine; DMPC, 1,2-dimyristoyl-*sn*-glycero-3-phosphocholine; DPC, dodecylphosphocholine; SLF, separated local field; TROSY, transverse relaxation optimized spectroscopy; PDB, Protein Data Bank; r.m.s.d., root mean square deviation.

electron due to its high redox potential as compared with ferric cytP450 (7–10). cytb$_5$ plays a key role in the oxidation of a variety of exogenous and endogenous compounds, including drugs, fatty acids, cholesterol, and sex hormones. The influence of cytb$_5$ on cytP450 activity has been shown to depend on the cytP450 isozyme and the substrate involved. Remarkably, cytb$_5$ enhances some catalytic reactions of cytP450 but does not affect or even inhibit others (6, 8–13). At low concentrations, cytb$_5$ may enhance the rate of catalysis by up to 100-fold, whereas at high concentrations it inhibits catalysis by competing with CPR for a binding site on cytP450, thereby preventing the transfer of the first electron and the reduction of ferric cytP450 to the ferrous form (6, 7, 14). cytb$_5$ and CPR are both negatively charged proteins, which are known to have overlapping binding sites on cytP450 (15). When the stimulatory and inhibitory effects of cytb$_5$ are equal, cytb$_5$ will appear to have no effect on the catalytic activity of cytP450.

To obtain an in-depth understanding of the molecular basis of the effects of cytb$_5$ on cytP450 activity, it is necessary to determine the structure of the complex between the full-length forms of cytb$_5$ and cytP450. Although all reported x-ray and NMR structural data pertain to cytosolic heme binding domains of truncated, microsomal cytP450 and cytb$_5$, in which their membrane anchors have been removed (16–19), neither structures nor dynamics of the full-length protein (containing the transmembrane domain) are currently available. Additionally, although the interaction of cytb$_5$ with various membranes has been previously studied (20–22), the structure of membrane-bound cytb$_5$ is lacking. However, only the full-length membrane-binding form of microsomal cytb$_5$ influences the enzymatic activity of cytP450 (23, 24); truncated cytb$_5$ is only capable of electron transfer to water-soluble oxidative enzymes (*e.g.* cytochrome *c* and metmyoglobin) (25).

Despite recent advances in NMR methodology and isotopic labeling schemes, the structure determination of large membrane-bound protein-protein (~70 kDa) complexes remains a monumental task. The large size of the membrane-bound complex presents considerable challenges in terms of sample stability, spectral sensitivity, and resolution. In this study, we present the first full-length tertiary structure of rabbit ferric[4] cytb$_5$ solved in a membrane mimetic using a combination of high resolution solution and solid-state NMR spectroscopy. Subsequently, experimentally derived restraints from NMR, site-directed mutagenesis, and double mutant cycle data, obtained on the full-length proteins, were then used to generate the structure of the complex between ferric microsomal rabbit cytP4502B4 (56 kDa) and cytb$_5$ (16 kDa), using a data-driven docking algorithm, HADDOCK (high ambiguity driven biomolecular docking) (26). The extensive structural knowledge of the cytb$_5$-cytP450 complex interface provided here will prove to be essential in unraveling the molecular mechanism by which cytb$_5$ regulates the rate of catalysis of cytP450 (14).

[4] Unless otherwise stated, all the NMR data were collected on the oxidized (ferric; Fe(III)) form of full-length cytP450 and cytb$_5$.

EXPERIMENTAL PROCEDURES

Materials—The QuikChange II XL site-directed mutagenesis kit was purchased from Stratagene. 1,2-Dilauroyl-*sn*-glycero-3-phosphocholine (DLPC) was purchased from Doosan Serdary Research Laboratories (Toronto, Canada), and methoxyflurane was obtained from Abbott. 1,2-Dihexanoyl-*sn*-glycero-3-phosphocholine (DHPC) and 1,2-dimyristoyl-*sn*-glycero-3-phosphocholine (DMPC) were purchased from Avanti Polar Lipids (Alabaster, AL). C41 cells were purchased from Lucigen (Middleton, MI). U-^{13}C-, U-^{2}H-, and U-^{15}N-labeled CELTONE rich media, U-^{15}N-CELTONE rich media, U-^{13}C,U-^{15}N-CELTONE-rich media, [^{2}H]dodecylphosphocholine (DPC-D38), [^{13}C]glucose, [^{15}N]ammonium sulfate, 2,2-dimethyl-2-silapentane-5-sulfonate, and D_2O were purchased from Cambridge Isotope Laboratories (Andover, MA). Resins, buffer components, and all chemicals, including BHT, benzphetamine and 1-CPI, were purchased from Sigma. Glycerol for NMR experiments was purchased from Sigma and Roche Applied Science. The NMR samples were placed into 5-mm symmetrical D_2O-matched Shigemi NMR microtubes (Shigemi, Inc., Alison Park, PA).

Generation of Mutants of cytP4502B4 and cytb$_5$—Mutagenesis was performed using a QuikChange II XL site-directed mutagenesis kit (Stratagene) according to the manufacturer's instructions. The oligonucleotides were synthesized by Integrated DNA Technologies. Following mutagenesis, the sequence of the entire mutated gene was determined at the University of Michigan DNA Sequence Core Facility to confirm the mutation and correct sequence.

Expression and Purification of Full-length Wild-type Rabbit cytP4502B4, Rat CPR, and Rabbit cytb$_5$—The cytP4502B4 and cytb$_5$ cDNA in pLW01 and CPR cDNA in pSC-CPR plasmids were expressed in *Escherichia coli* C41 cells and purified as described previously (15, 27, 28). [U-^{15}N]cytb$_5$, [U-^{13}C,U-^{15}N]cytb$_5$, and [U-^{13}C,U-^{2}H,U-^{15}N]cytb$_5$ were expressed using Celtone-N, Celtone-CN, and Celtone-DCN complete media, respectively, with additional supplements as described previously (29). Prior to expressing [U-^{13}C,U-^{2}H,U-^{15}N]cytb$_5$, C41 cells containing pLW01-cytb$_5$ plasmid were adapted to grow in 100% Lysogeny Broth (LB) media by gradually increasing the D_2O concentration in the LB medium from 10, 30, 60, and 80 to 100% D_2O. After each successive cycle, an LB culture was inoculated with three colonies that had been grown on a plate containing a lower amount of D_2O. The liquid culture with the higher amount of D_2O was incubated for up to ~8 h at 37 °C with shaking at 250 rpm. 50 μl of the resulting culture was plated on an LB agar plate containing 0.24 mM carbenicillin and the higher D_2O concentration. This process was repeated until the cells were able to grow on LB plates containing 100% D_2O. The protocols for the expression of [U-^{13}C,U-^{2}H,U-^{15}N]cytb$_5$, [U-^{13}C,U-^{15}N]cytb$_5$, and [U-^{15}N]cytb$_5$ were identical; however, the cells were harvested at different times as follows: for [U-^{15}N]cytb$_5$ and [U-^{13}C,U-^{15}N]cytb$_5$, the cells were harvested after 20 h of incubation at 35 °C with shaking at 200 rpm, and for [U-^{13}C,U-^{2}H,U-^{15}N]cytb$_5$, cells were harvested after 48 h. Purification of cytb$_5$, cytP450, and CPR was performed as described elsewhere (15, 28). Each purified protein

exhibited a single band on an SDS-polyacrylamide gel (data not shown). CytP450 concentration was quantified by the method of Omura and Sato (30).

Solution NMR Data Collection—All NMR experiments were performed at 298 K on a Bruker Avance 900 MHz four-channel NMR system equipped with an *x,y,z* axis PFG 5-mm TCI cryoprobe. Samples for NMR were prepared using an appropriate amount of protein (0.1–0.5 mM) in 100 mM potassium phosphate buffer at pH 7.4 and 5% (w/v) glycerol (referred to as NMR buffer) incorporated into either deuterated dodecylphosphocholine (DPC-D38, 45 mM) micelles or lipid isotropic bicelles composed of DMPC and DHPC lipids (DMPC/DHPC = q ratio of 0.25). Protein NMR samples in isotropic bicelles were prepared such that the final lipid concentration was 10% (w/v), and the DMPC and DHPC lipid ratio was 1:4 (as described previously (29)).

Sequence-specific Assignment of cytb$_5$—^{1}HN, ^{15}N, ^{13}Cα, ^{13}Cβ, and ^{13}CO backbone resonances was achieved using a set of TROSY-based three-dimensional HNCO, HN(CA)CO, HNCA, HN(CO)CA, and HNCACB experiments. Intra-residue, inter-residue, and sequential NOEs were obtained from three-dimensional ^{15}N HSQC-NOESY and ^{13}C HSQC-NOESY spectra on fully protonated and uniformly ^{15}N- and ^{13}C-labeled cytb$_5$ in DPC-D38 micelles; these experiments were conducted at optimal mixing times of 80 and 100 ms, respectively. ^{15}N HSQC-TOCSY spectrum was also collected to assist in the assignment of intra-residue NOEs. All aromatic side chain protons and carbon atoms were assigned using two- and three-dimensional NOESY. The proton chemical shift was referenced at 0.0 ppm to the methyl signal of 2,2-dimethyl-2-silapentane-5-sulfonate as an internal reference. The ^{13}C and ^{15}N chemical shifts were referenced indirectly to 2,2-dimethyl-2-silapentane-5-sulfonate (31). All NMR spectra were processed using either NMRPipe (32) or TopSpin 2.0 (Bruker). Sequential and NOE assignments were made using Sparky (33).

Structure Determination of Heme Domain of cytb$_5$—Initial restraints for the backbone torsion angles ϕ and ψ were obtained from chemical shifts using TALOS (34), provided as part of the NMRPipe package (32), and NOE patterns. The upper bound for all NOE distance restraints was initially set to 5 Å and adjusted for nonstereospecific assignment of methylene and methyl protons using the method described originally for DYANA (35). The structure calculations were performed with CYANA 2.1 (36), which uses simulated annealing in combination with molecular dynamics in torsion angle space. Chemical shift tolerances of 0.02, 0.3, and 0.45 ppm were used for ^{1}H, ^{13}C, and ^{15}N, respectively. For initial structure calculations, only unambiguous peak assignments, obtained from three-dimensional NOESY, were used. More than 90% of these peaks were assigned manually, and the remaining peaks were assigned using CYANA 2.1 (36). Using these assignments and TALOS-derived torsion angle restraints, an initial ensemble of NMR structures was generated. Initial violated restraints were identified and eliminated in subsequent rounds of structure calculations until a consistent set of restraints was obtained with no violations greater than 0.2 Å in the ensemble (Table 1). Starting *ab initio*, 100 conformers were calculated in 10,000 annealing steps each. PyMOL (Version 1.1, Schrödinger, LLC) was used to visualize the resulting ensemble of energy-minimized conformers.

TABLE 1
NMR resonance assignments, constraints and refinement statistics for the cytb$_5$ structure

NMR distance and dihedral constraints	
Distance constraints	
Total NOE	1787
Intra-residue	377
Inter-residue	
Sequential ($\|i-j\|=1$)	513
Medium range ($\|i-j\|<4$)	412
Long range ($\|i-j\|>5$)	485
Hydrogen bonds	39
Total dihedral angle restraints	
ϕ	56
ψ	56
Violations	
Max. dihedral angle violation (>2°)	0
Max. distance constraints violation (>0.2 Å)	0
Ramachandran analysis	
Most favored	71.70%
Allowed	25.90%
Generously	2.30%
Disallowed	0.00%
Average r.m.s.d. (Å)	
Backbone (Lys-7--Arg-89)	0.32 ± 0.10
Heavy (Lys-7--Arg-89)	0.82 ± 0.10

Solid-state NMR of cytb$_5$—Magnetically aligned DMPC/DHPC bicelles, with a molar ratio of DMPC to DHPC of 3.5:1 and a weight percentage of lipid of 30% (w/v), containing uniformly ^{15}N-labeled cytb$_5$ were prepared as described elsewhere (29). A two-dimensional separated local field (SLF) NMR experiment using the HIMSELF (heteronuclear isotropic mixing leading to spin exchange via the local field) (37) pulse sequence, which is based on the PIWIMz (polarization inversion by windowless isotropic mixing) pulse scheme, was obtained at 310 K using a ramped cross-polarization contact time of 0.8 ms, 2 s recycle delay and 32 t_1 increments. Radio frequency field strengths of 50 and 35 kHz were used for the WIM (windowless mixing) (38) sequence during t_1 and SPINAL-64 (39) decoupling during acquisition, respectively.

Docking of Heme into cytb$_5$ NMR Structure—HADDOCK 2.1 (26, 40) was used to incorporate the heme molecule (type B) into the 20 NMR-derived low energy structures of cytb$_5$ presented here. Unambiguous restraints were compiled based on distances (between the heme and certain cytb$_5$ residues) measured from the available crystal structure of cytb$_5$ (PDB code 1DO9) (18). As a first step, rigid body energy minimization was used for docking 2000 structures. The second step included semi-rigid simulated annealing, and the best 500 structures were selected for refinement. The best 200 structures were then selected for final refinement with explicit solvent in an 8.0-Å shell of TIP3P water molecules. The 50 lowest energy structures were then subjected to a detailed analysis.

Solution NMR of cytb$_5$-cytP450 Complex—Samples containing a 1:1 molar complex of 0.1 mM isotopically ^{15}N-labeled ferric cytb$_5$ and unlabeled ferric cytP450 in NMR buffer were prepared. For solution NMR measurements, isotropic bicelles were added to the complex sample just before transferring to a Shigemi tube. For experiments in the presence of the substrate and inhibitor (BHT and 1-CPI), the small molecule was added to cytP450 to a final concentration of 0.2 mM (1:2 molar ratio for

cytP450/substrate) before the addition of isotropic bicelles. To assess the formation of the cytb$_5$-cytP450 complex, three cytP450 titration points were performed. All titrations points were carried out by adding aliquots of unlabeled cytP450 solution to a final concentration of 0.03, 0.06, and 0.10 mM into a sample, containing 0.1 mM ^{15}N-labeled cytb$_5$ and 0.2 mM BHT in isotropic bicelles.

SDS-PAGE of the cytb$_5$-cytP450 complex incorporated in bicelles was performed before and after NMR experiments to ensure that proteolysis, especially of the membrane anchor of cytb$_5$, had not occurred during the experiments (data not shown). The proteins were full-length both before and after NMR measurements. In addition, carbon monoxide (CO) difference spectra of cytP4502B4, and activity assays of cytb$_5$ and cytP4502B4 (supplemental Table S1), confirmed the presence of the functional form of cytP450 and the cytb$_5$-cytP450 complex in the NMR samples(data not shown).

Determination of cytb$_5$-cytP450 Equilibrium Dissociation Constant (K_d) in the Presence of a Substrate/Ligand—The K_d value of the binding between ferric cytP4502B4 and ferric cytb$_5$ was determined as described previously (15) by measuring the type I spectral change (a decrease at 420 nm and an increase at 385 nm in absorption) occurring when cytb$_5$ is added to an aqueous solution of cytP4502B4, in the presence of the substrate, methoxyflurane, or BHT. The K_d value was used to calculate the free energy of binding, ΔG, using the formula $\Delta G = -RT\ln(K_d)$, where R is the gas constant and T is temperature. The K_d value for the complex formation of all possible pairs of wild type and mutants combinations of cytP4502B4 and cytb$_5$ was determined as described previously (15) and are presented in Tables 3 and 4. The K_d value could not be calculated in the presence of either micelles or bicelles.

Activity of cytP4502B4 in Solution and Bicelles, Methoxyflurane—The metabolism of the anesthetic, methoxyflurane ($C_3H_4Cl_2F_2O$), by cytP4502B4 was measured in a reconstituted aqueous system with and without cytb$_5$ (23). The activity of cytP450 was also measured in bicelles in the presence and absence of cytb$_5$. The activity was quantified by recording the amount of fluoride ion produced. The components were mixed together in the following sequence: cytP4502B4, CPR, and DLPC. The mixture was then incubated for 5 min at room temperature, and either cytb$_5$ or buffer was added to the mixture, which was then incubated for an additional 1 h at room temperature. Following the 1-h incubation, 50 mM potassium phosphate buffer of pH 7.4 saturated with methoxyflurane (1 μl/ml), glucose 6-phosphate, and glucose-6-phosphate dehydrogenase were added, and the solution was further incubated at 37 °C for 5 min. NADPH was added to start the reaction. The final volume of the reaction mixture was 500 μl, and it contained 50 mM potassium phosphate buffer, 1 μM cytP4502B4, 1 μM CPR, 120 μM DLPC, 1 μl/ml methoxyflurane, 300 μM NADPH, 5 mM glucose 6-phosphate, 1 unit/ml glucose-6-phosphate dehydrogenase, and cytb$_5$ (0 or 1 μM). The resulting reaction mixture was incubated at 37 °C with shaking at 150 rpm for 30 min and then quenched by heating at 70 °C for 2 min. The fluoride ion concentration of the solution was quantified using a fluoride ion electrode (Thermo Scientific).

The assay for the metabolism of methoxyflurane in the presence of bicelles was conducted as described above except that the cytP450-CPR-cytb$_5$ complex was added to DMPC/DHPC (3.5/1) bicelles at 4 °C. Bicelles were prepared and precooled as described previously (29). The mixture was incubated at 4 °C for 30 min. The potassium phosphate buffer saturated with methoxyflurane was added to the protein mixture. The resulting mixture was incubated at 37 °C for 5 min at which time NADPH was added to a final concentration of 300 μM to start the reaction. The final concentration of DMPC was 110 mM. The results of the methoxyflurane assay are presented in supplemental Table S1.

Benzphetamine—The metabolism of benzphetamine was measured by determining the amount of formaldehyde produced by the *N*-demethylation of benzphetamine using Nash's reagent, as described previously (15). The final concentration of the reactants in the mixture was 50 mM potassium phosphate buffer (pH 7.4), 0.2 μM cytP4502B4, 0.2 μM CPR, 24 μM DLPC, 1 mM benzphetamine, 300 μM NADPH, 0 or 50 mM DMPC/DHPC bicelles, and cytb$_5$ (0 or 0.2 μM). The results of the benzphetamine assays are presented in supplemental Table S1.

cytb$_5$-cytP450 Complex Structure Calculation—HADDOCK 2.1 (26) algorithm was used to dock cytb$_5$ and cytP450 based on four unambiguous restraints derived from the double mutant cycle analysis and a number of ambiguous restraints derived from NMR and site-directed mutagenesis experiments (Table 5). HADDOCK involves rigid body docking, followed by molecular dynamics simulations that allow selected amino acid side chains, as well as parts of the backbone, to move freely to improve the complementarity and electrostatic interactions at the interface. For this calculation, we used our solution NMR structure of rabbit cytb$_5$ (Met-1 to Ser-105 of PDB structure 2M33, the transmembrane domain was not taken into consideration for the simulations) and the x-ray structure of the heme domain of cytP4502B4 lacking the transmembrane anchor (PDB code 1SUO (41)). HADDOCK was run using the default parameters. Ligand topology and parameter files were generated from the PRODRG2 server (42). Rigid body energy minimization was used for docking 2000 structures of the complex. The second step included semi-rigid simulated annealing from which the best 500 structures were selected for refinement. The best 150 structures were further refined with explicit solvent in an 8.0 Å shell of TIP3P water molecules. The 50 lowest energy structures were selected for the final analysis and grouped into two main clusters based on the backbone r.m.s.d. The interface of the complex was analyzed by PISA (polarity index slant angle) (43) and Collaborative Computational Project Number 4 (44), and molecular graphics were prepared using PyMOL (Version 1.1).

RESULTS

Rabbit cytb$_5$ is composed of a large cytosolic heme domain and a C-terminal transmembrane domain, connected by a 15-residue linker. To identify cytb$_5$ residues involved in complex formation with cytP4502B4, we first solved the three-dimensional structure of ferric cytb$_5$ in DPC micelles, using a combination of high resolution solution and solid-state NMR experiments (Fig. 1).

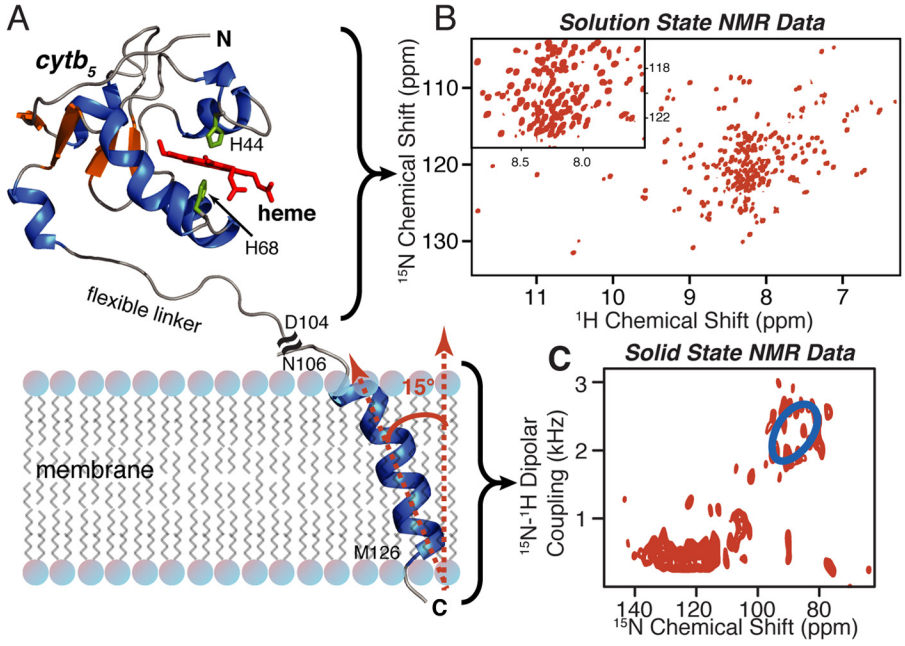

FIGURE 1. **NMR structure of rabbit microsomal cytb$_5$.** *A*, NMR structure of full-length cytb$_5$ obtained from a combined solution and solid-state NMR approach. The soluble heme domain structure (residues 1–104) of full-length cytb$_5$ was solved in DPC micelles by solution NMR, with a backbone r.m.s.d. of 0.32 ± 0.10 Å. The transmembrane domain structure (residues 106–126) of full-length cytb$_5$ was determined in aligned DMPC/DHPC bicelles using solid-state NMR spectroscopy. *B*, ^{1}H-^{15}N TROSY-HSQC spectrum of uniformly, ^{13}C-, ^{2}H-, and ^{15}N-labeled cytb$_5$ in micelles exhibiting well resolved peaks. *C*, two-dimensional HIMSELF spectrum of uniformly ^{15}N-labeled cytb$_5$ reconstituted in aligned DMPC/DHPC bicelles. The *blue ring* presents the best fit for the helical wheel pattern of resonances from the α-helical transmembrane domain of cytb$_5$.

Three-dimensional Structure Determination of Full-length Mammalian cytb$_5$—Isotopically labeled full-length wild-type ferric microsomal rabbit cytb$_5$ was reconstituted in detergent (DPC) micelles. A number of standard TROSY-based multidimensional solution NMR experiments, in combination with isotopic labeling schemes, including perdeuteration, were employed to assist in resonance assignment and structure determination of cytb$_5$. Fig. 2 presents a ^{1}H-^{15}N TROSY-HSQC spectrum of U-^{13}C-, U-^{2}H-, and U-^{15}N-labeled full-length wild-type cytb$_5$ incorporated in DPC micelles at 25 °C. The spectrum exhibits well resolved and dispersed NH correlations from cytb$_5$ residues, suggesting that the protein is well folded and monodispersed in DPC micelles.

Using standard three-dimensional solution NMR experiments, NMR resonance assignment was achieved for 88.5% of the backbone and side chain atoms of residues from the soluble domain of full-length cytb$_5$ (Table 2). The chemical shift assignments were deposited in the Biological Magnetic Resonance Bank (code 18919). An inspection of the ^{1}H-^{15}N TROSY-HSQC spectrum of cytb$_5$ revealed two or more NMR resonances for many of the residues. These two sets of NMR resonances originate from the two isomers (major and minor) of cytb$_5$ that differ by a 180° rotation of the heme plane about the axis that cuts through the *meso*-carbon atoms α and γ (18, 45). The ratio of the populations of the two isomers can be calculated by determining the peak intensity ratio (here in the ^{1}H-^{15}N TROSY-HSQC spectrum of cytb$_5$) for identical residues in the two isomeric forms. The major/minor isomer ratio in our study for full-length rabbit cytb$_5$ was determined to be about 6.6:1 which is similar to 5:1 ratio previously obtained for truncated rabbit cytb$_5$ (18) and nearly identical to the isomer ratio of 6.5:1 for truncated bovine cytb$_5$ (45). The ratio depends

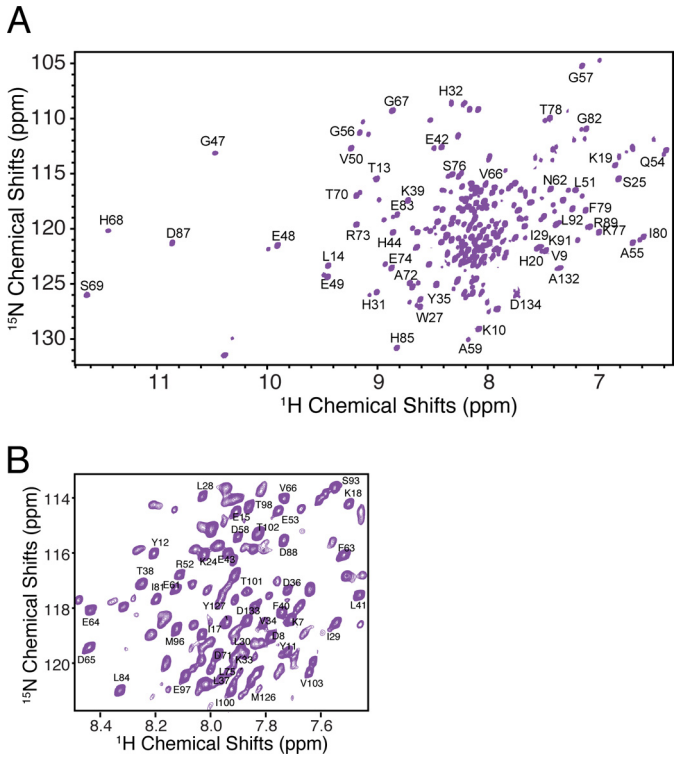

FIGURE 2. **High resolution solution NMR spectrum of cytb$_5$.** *A*, ^{1}H-^{15}N TROSY-HSQC spectrum of uniformly ^{13}C-, ^{2}H-, and ^{15}N-labeled full-length mammalian cytb$_5$ in DPC micelles. The backbone resonance peaks are labeled with the residue-specific assignment of cytb$_5$. Unlabeled peaks include side chain resonances (Asn, Gln) and the lower populated cytb$_5$ isomer. Tryptophan indole protons between 10 and 11 ppm were not assigned due to broadening. *B*, expansion of the crowded region of the ^{1}H-^{15}N TROSY-HSQC spectrum.

TABLE 2

Protein NMR resonance assignment for the backbone and side chain atoms of cytb$_5$

Residues 1–105 form the heme domain and the linker region, and residues 106–134 form the transmembrane domain of cytb$_5$.

Cytb5 unambiguous backbone assignments for non-proline residues are as follows: 7–22, 24–32, 34–90, 92, 93, 96–99, and 101–104 (heme domain) and 106, 127, 133, and 134 (transmembrane domain)
Cytb5-ambiguous backbone assignments as follows: 124, 126, and 128
Residues with no assignments (non-proline residues) as follows: 1–6, 23, 33, 91, 94, 100, 105, 107–123, 125, and 129–132
Proline residues as follows: 45, 86, 95, and 116

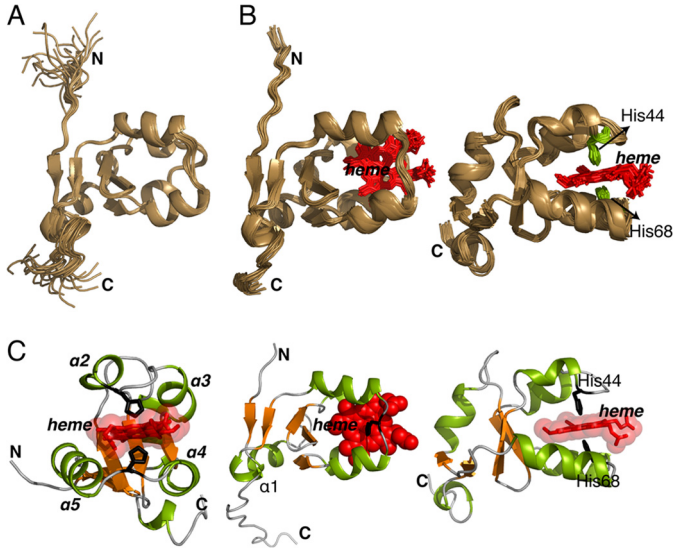

FIGURE 3. **Solution NMR structure of the cytosolic domain of full-length cytb$_5$ in DPC micelles.** *A,* overlay of the 20 lowest energy structures of cytb$_5$ generated from CYANA2.1 based on the NMR restraints in Table 1. The backbone (Lys-7 to Arg-89) r.m.s.d. was 0.32 Å. *B,* two different views of the overlay of the 20 lowest energy structures of the heme domain of cytb$_5$ generated from HADDOCK after docking heme B. His-44 and His-68, which coordinate the heme, are represented as *green sticks*. *C,* three different views of the structure of the heme domain of cytb$_5$ obtained from solution NMR, with the heme B molecule orientation obtained from HADDOCK. *Left, middle,* and *right* orientations show the proximal, bottom (lower edge of the cleft), and side view of cytb$_5$, respectively.

on the cytb$_5$ species and has been reported to be as high as 1.5:1 for rat cytb$_5$ (46), despite the sequence similarity between rat and rabbit cytb$_5$ (supplemental Fig. S1*A*). Although backbone assignments were done for the resonance peaks of both the major and minor isomers, all structure analyses were performed for the major isomer of ferric cytb$_5$.

NMR resonance assignments of the major isomer of cytb$_5$ in DPC micelles revealed that the observed ^{1}H-^{15}N TROSY-HSQC spectrum is dominated by resonances from the soluble heme-containing domain and the flexible linker of cytb$_5$ (Fig. 2). Residues from the transmembrane domain of cytb$_5$ could not be identified in the ^{1}H-^{15}N TROSY-HSQC spectrum (Table 2). To identify the origin of the lack of transmembrane domain resonances in solution NMR, and to determine the structure and topology of the transmembrane domain of cytb$_5$, solid-state NMR was performed on full-length cytb$_5$ incorporated in aligned DMPC/DHPC bicelles (explained below). It is important to note here that the full-length form of cytb$_5$ incorporated in a membrane mimetic (DPC micelles or lipid bicelles) was used for all solution and solid-state NMR measurements.

Three-dimensional Tertiary Structure Calculation of the Heme Domain of Full-length cytb$_5$—A high resolution structure of the soluble domain of the major isomer of full-length ferric cytb$_5$ (~16 kDa) in DPC micelles was calculated using a total of 1787 NOE restraints (Table 1). Distances derived from NOE restraints, in conjunction with 39 hydrogen bonds and 112 (ϕ and ψ) dihedral angles, were included for structural determination into CYANA 2.1 (36). Twenty minimum energy conformers (Fig. 3*A*) of cytb$_5$ with backbone and heavy atom (residues Lys-7 to Arg-89) r.m.s.d. values of 0.32 ± 0.10 and 0.82 ± 0.10 Å, respectively, were selected from 100 structures calculated in 10,000 annealing steps. Distance restraints used for the structural calculation and Ramachandran statistics can be found in Table 1. HADDOCK 2.1 was used to dock heme B into the 20 NMR-derived low energy structures of cytb$_5$ (see "Experimental Procedures") (26, 40). Fifty low energy structures were obtained with no restraint violations. The 20 lowest energy HADDOCK-generated structures of cytb$_5$ (Fig. 3) were deposited in the Protein Data Bank (code 2M33). This solution NMR structure of cytb$_5$ was used in all subsequent analyses.

The structure of cytb$_5$ contains five α-helices, five β-strands, and one 3_{10} helix (Fig. 3*C* and supplemental Fig. S1). The first β-sheet is observed for residues Lys-10 to Tyr-12 with an α-helix (α1, Leu-14 to Hi-s20) following shortly after. The heme-binding portion of cytb$_5$ consists of two helices in the lower cleft, labeled as α4 (Thr-60 to Val-66) and α5 (Thr-70 to Phe-79), two helices in the upper cleft, labeled as α2 (Lys-39 to Glu-43) and α3 (Glu-49 to Gln-54) (Fig. 3C), and three β-strands at the bottom of the heme pocket, labeled as β3 (Lys-33 to Asp-36), β2 (Trp-27 to Leu-30), and β4 (Gly-56 to Asp-58). At the end of the structured soluble domain lies a β-strand (β5, Gly-82 to Leu-84) and a 3_{10} helix (Pro-86 to Arg-89). The overall structure of the heme domain of full-length ferric cytb$_5$ is found to be similar to the previously determined NMR structure of the heme domain of truncated ferric cytb$_5$ from rabbit (18).

Flexible Linker Domain of cytb$_5$ Lacks a Defined Secondary Structure—The linker region (Ser-90–Asp-104), which connects the cytosolic heme domain of cytb$_5$ to the transmembrane anchor, was previously characterized as random coil for various truncated forms of microsomal cytb$_5$ that lacked a transmembrane domain (18, 19); in these proteins, the C terminus had been truncated either within the linker region or beyond it. Neither intra- nor inter-residue NOEs were observed for most of the linker residues (Ser-90 to Asp-104) due to the rapid solvent exchange at those amide positions. Therefore, we show here that for full-length cytb$_5$, incorporated in DPC micelles, the linker region is unstructured, lacking any distinct secondary structural features. A cytb$_5$ linker region of at least 6–8 amino acids has been shown to be necessary to enable formation of a functional complex between cytb$_5$ and its full-length redox partner cytP450 (23). Unlike full-length cytb$_5$, a cytb$_5$ mutant lacking eight amino acids in the linker domain was neither able to insert efficiently into a lipid membrane (47) nor able to form a fully functional complex with cytP450 (23). The extended form of the cytb$_5$ linker region, presented here, should provide the flexibility and orientational freedom necessary for efficient complex formation with its redox partners.

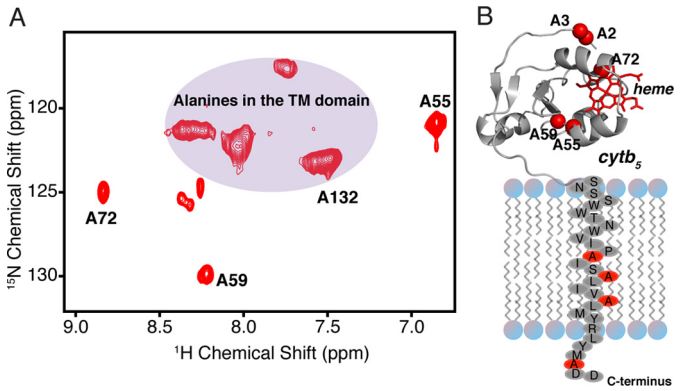

FIGURE 4. **Transmembrane domain of cytb$_5$ is visible under magic angle spinning NMR.** *A,* ^{1}H-^{15}N-HMQC spectrum recorded on a selectively [^{15}N]alanine-labeled sample of cytb$_5$ incorporated in DPC micelles. This spectrum was obtained from a 600 MHz Varian solid-state NMR spectrometer under a 2.5 kHz spinning speed of the sample at 37 °C, using a double-resonance magic angle spinning nanoprobe (Agilent/Varian). *B,* representation of cytb$_5$ highlighting all the alanines (*red sphere*) in the protein.

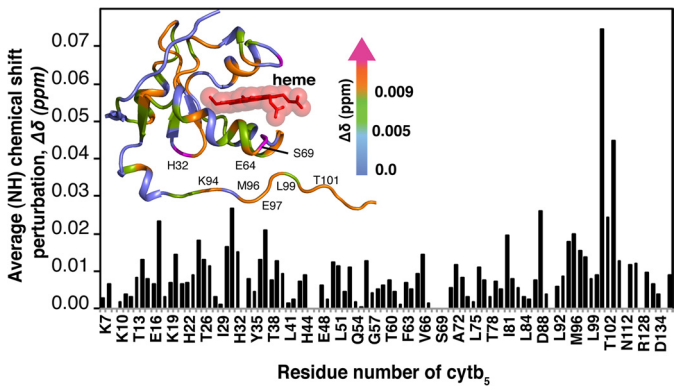

FIGURE 5. **Chemical shift perturbation analysis.** A histogram presenting the experimentally measured changes in chemical shift values for residues in cytb$_5$ upon complex formation with cytP450. The change in the chemical shift was calculated using the standard formula $\Delta\delta = \sqrt{\{(\omega_{HN}\Delta^{1}HN)^2 + (\omega_N\Delta^{15}N)^2\}}$, where $\omega_H = 1$, $\omega_N = 0.154$, and $\Delta\delta$ represents the average (NH) chemical shift perturbation (82). The chemical shift perturbations are represented as a continuous *color map* on the NMR structure of cytb$_5$. Resonances for His-32, Gly-46, His-68, and Ser-69 (represented in *magenta*) disappear upon complex formation.

Structure of the Soluble Domain of cytb$_5$ Is Unaffected by Its Membrane Environment—The ^{1}H-^{15}N TROSY-HSQC spectrum was also obtained for full-length cytb$_5$ in 10% (w/v) DMPC/DHPC isotropic bicelles with a *q* ratio of 0.25. The majority of the spectrum was nearly identical to the one obtained in DPC micelles (data not shown). The largest chemical shift changes were observed for the tryptophan indole side chain (NH) resonances of Trp-109, Trp-110, and Trp-113 residues. These tryptophan residues are predicted to be at the edge of the transmembrane domain and hence should be most affected by the change in the membrane environment when going from micelles to lipid bicelles.

Establishing the Topology and Structure of the Transmembrane Domain of Full-length cytb$_5$ in Bicelles—As mentioned above, the resonances for residues in the transmembrane domain of cytb$_5$, reconstituted in either isotropic bicelles (DMPC/DHPC) or DPC micelles, were not identified in the ^{1}H-^{15}N TROSY-HSQC solution NMR spectra. Although sequential NOE assignments could not be carried out for the residues in the transmembrane domain, ambiguous NOE assignments, without secondary structural information, were possible for the Hα and side chain protons of residues Asn-121 to Asp-134 in solution NMR. A ^{1}H-^{15}N-HMQC spectrum recorded under magic angle spinning (2.5 kHz) on a selectively [^{15}N]alanine-labeled sample of cytb$_5$ incorporated in DPC micelles displayed broad resonances for the backbone amide-NHs of the four alanines present in the transmembrane domain of cytb$_5$, along with narrow resonances for the alanines in the soluble domain (Fig. 4). These data suggest that the restricted motion of the transmembrane domain of cytb$_5$ incorporated in a DPC micelle, or isotropic bicelles, causes significant broadening of the transmembrane domain resonances due to fast spin-spin relaxation. To obtain the structure of the transmembrane domain of cytb$_5$, we employed an alternative technique of static solid-state NMR spectroscopy on uniformly ^{15}N-labeled full-length cytb$_5$ incorporated in bicelles (48, 49) composed of DMPC and DHPC lipids in a 3.5:1 molar ratio, which were magnetically aligned in the external magnetic field.

A two-dimensional SLF NMR experiment using the HIMSELF (29) pulse sequence, which is based on the PIWIMz pulse scheme, was performed on magnetically aligned bicelles containing cytb$_5$ (Fig. 1*C*). The resultant two-dimensional SLF spectrum correlates ^{15}N chemical shifts with ^{1}H-^{15}N dipolar couplings. The two-dimensional spectrum in Fig. 1*C* exhibits a distinct circular PISA-wheel pattern of resonances between 60 and 100 ppm, which is indicative of an α-helical conformation and was assigned to the transmembrane anchor of cytb$_5$ based on our previous work (29, 50). This is in agreement with previous circular dichroism (51) and Fourier transform infrared (52) experiments, which indicated that the transmembrane domain is at least 50% helical.

The observed PISA wheel was empirically fitted (53) to determine the average tilt angle of the transmembrane α-helix with respect to the bilayer normal. The resonance pattern was consistent with an average tilt of 15 ± 3°, in agreement with our previously published work (29). The value of the helix's order parameter was estimated to be 0.86. Additionally, a "structure fitting algorithm" (54) was used in combination with the solid-state SLF NMR data to determine the backbone structure of the transmembrane anchor as a whole, as presented in Fig. 1*A*. Interestingly, the transmembrane domain of cytb$_5$ is conserved among vertebrates (sequence similarity of 78–96% (23)) and is essential for complex formation with redox partners (55); both suggest that this α-helical domain plays an important role in the function of cytb$_5$ and its interactions with redox partners.

cytP4502B4-binding Epitope on cytb$_5$ by NMR—Perturbations in the amide-NH chemical shifts (Fig. 5) and peak heights (Fig. 6) of ^{15}N-labeled full-length ferric cytb$_5$ upon complex formation with unlabeled full-length ferric cytP4502B4 in isotropic bicelles composed of DMPC and DHPC lipids (DMPC/DHPC = *q* ratio of 0.25) were measured to identify the binding cytb$_5$ epitope for cytP450. The addition of cytP450 to cytb$_5$ in an equimolar ratio had two effects as follows: (*a*) it caused an overall reduction of the cytb$_5$ amide signal intensities, indicating complex formation between cytP450 and cytb$_5$, which increases the overall correlation time of cytb$_5$ (Fig. 6*A*, *yellow*

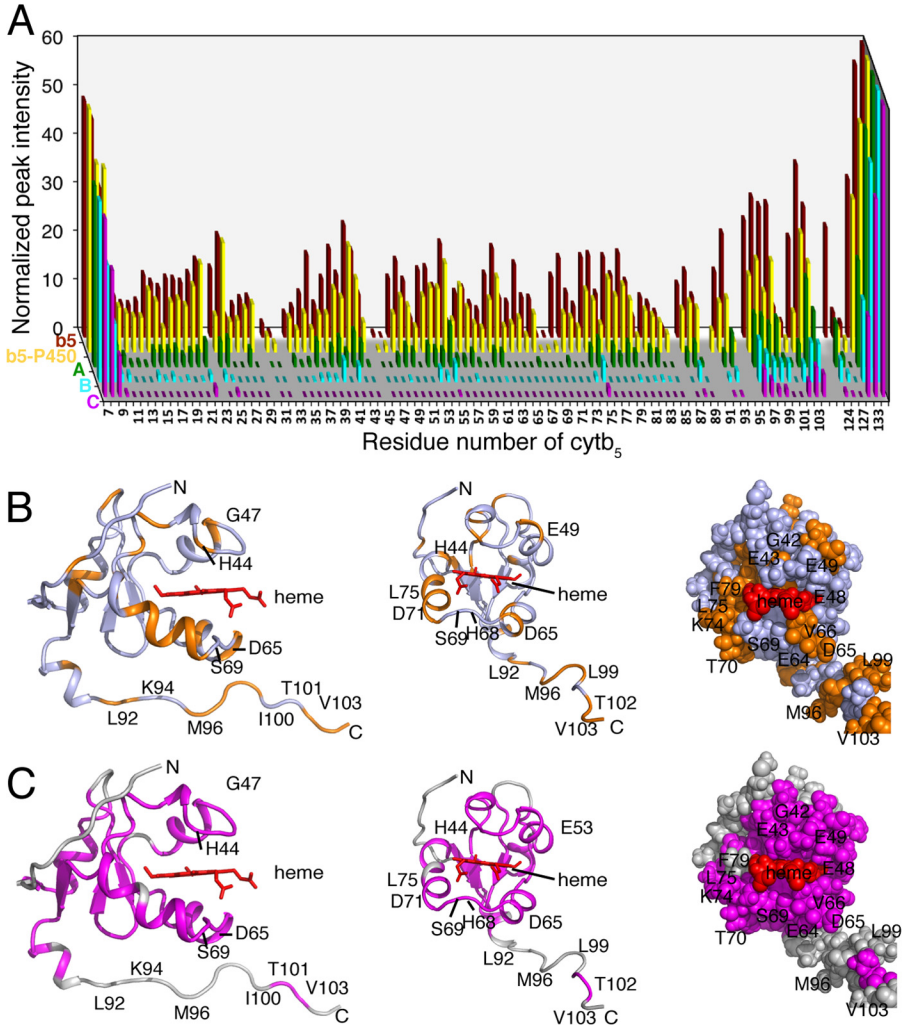

FIGURE 6. **Mapping the effect of cytP450 binding to cytb$_5$ measured from NMR.** *A,* histogram representing the differential line broadening NMR data for the cytb$_5$-cytP450 complex. The amide peak intensities for free cytb$_5$ are presented in *red*. *Yellow* presents the intensities for cytb$_5$ residues in a 1:1 equimolar complex with substrate-free cytP450. *Green, cyan,* and *magenta* highlight the extensive peak broadening observed for cytb$_5$ residues upon addition of the increasing amounts of unlabeled cytP450 bound to BHT (A = 1:0.3, B = 1:0.6, and C = 1:1 molar ratios between cytb$_5$ and cytP450). All peak intensities were normalized to the C-terminal residue Asp-134 in the unbound cytb$_5$ spectrum to account for the change in intensity upon complex formation. *B* and *C* present two different views of cytb$_5$ rotated by 90° with respect to each other and a space-filling representation of the second view. *B,* cytb$_5$ residues exhibiting extensive line broadening (with a decrease in peak height >20% as compared with free cytb$_5$) upon complex formation with an equimolar amount of substrate/ligand-free cytP450 are colored *orange* onto the NMR structure of cytb$_5$. *C,* residues of cytb$_5$ whose resonances are broadened beyond detection upon complex formation with an equimolar amount of cytP450 bound to BHT are represented in *magenta*. All NMR data were collected on the full-length complex incorporated in isotropic bicelles.

histogram), and (*b*) it caused modest chemical shift perturbations for cytb$_5$ backbone amide resonances.

A histogram depicting the weighted average chemical shift perturbations ($\Delta\delta$) observed for residues of cytb$_5$ upon complex formation with cytP450 is presented in Fig. 5. The average chemical shift perturbations observed for the backbone amides of cytb$_5$, upon addition of cytP450, are relatively small in magnitude, <0.01 ppm, and are spread over a large area of cytb$_5$. As a result, no specific regions of cytb$_5$ can be highlighted as being part of the interaction epitope, based on chemical shift perturbations. This lack of widespread changes in chemical shifts across the ^{1}H-^{15}N TROSY-HSQC spectrum indicates that there is no notable change in the overall tertiary fold of cytb$_5$ upon interaction with cytP450.

The reason for the small average chemical shift perturbations could be 2-fold. First, fast-to-intermediate (ns-μs) chemical exchange between the free observable cytb$_5$ in isotropic bicelles and the unobservable high molecular weight bound-state of the cytb$_5$-cytP450 complex in isotropic bicelles (> 100 kDa) (56, 57) would explain the overall broadening of the observed cytb$_5$ resonances. Our findings are in agreement with a recent NMR study, where they observed very modest chemical shift perturbations upon complex formation between truncated forms of cytP45017A1 and human cytb$_5$ lacking the membrane domains (58). Second, small and widespread chemical shift perturbations could be a result of the formation of an ensemble of dynamic "encounter complexes" as have been reported previously for other metalloprotein complexes (56, 59–62) such as cytb$_5$-myoglobin (56, 57). Encounter complexes are composed of an ensemble of protein orientations within the complex; this leads to very small chemical shift perturbations as observed for the cytb$_5$-cytP450 complex here and for other redox partners previously (56).

TABLE 3
K_d values and methoxyflurane metabolism of cytb$_5$-cytP450 complexes, determined with both wild-type and mutant proteins

cytb$_5$ or cytP450 mutants	K_d cytb$_5$-cytP450 complex (μM ± S.D.)	Methoxyflurane metabolism (nmol of F^- formed per min/nmol P450 ± S.D.)	Ratio of activity ± cytb$_5$
cytb$_5$ mutants			
No cytb$_5$ (control)		0.19 ± 0.2	
Wild-type cytb$_5$	0.022 ± 0.003	1.35 ± 0.02	7.1
E42A	0.012 ± 0.002	1.10 ± 0.1	5.8
E43A	0.015 ± 0.003	1.41 ± 0.2	7.4
E49A	0.032 ± 0.004	1.17 ± 0.2	6.2
V50A	0.016 ± 0.001	1.08 ± 0.2	5.7
N62A	0.010 ± 0.004	0.92 ± 0.1	4.8
D65A	0.332 ± 0.033	0.22 ± 0.02	1.1
V66A	0.152 ± 0.019	0.77 ± 0.1	4.1
D71A	0.017 ± 0.008	1.66 ± 0.2	8.7
cytP4502B4 mutants			
Wild-type cytP450	0.022 ± 0.003	1.32 ± 0.02	8.3
R122A	0.221 ± 0.06	0.54 ± 0.03	3.4
R126A	0.453 ± 0.06	0.19 ± 0.1	1.2
R133A	1.502 ± 0.18	0.06 ± 0.1	0.29
F135A	0.205 ± 0.05	0.43 ± 0.1	2.7
M137A	0.379 ± 0.07	0.33 ± 0.2	1.7
K139A	0.611 ± 0.13	0.12 ± 0.2	0.75
K433A	0.458 ± 0.04	0.05 ± 0.01	0.31
H226A	0.032 ± 0.009	1.37 ± 0.3	8.5

A closer inspection of Fig. 6*A* reveals differential line broadening of cytb$_5$ resonances upon complex formation with substrate-free cytP450 (*yellow*). The line broadening could be the result of the following: (*a*) changes in chemical shifts suggesting a conformational change in the protein or (*b*) a change in the transverse relaxation rate of cytb$_5$ resonances caused by a direct interaction with cytP450 (63). The absence of significant chemical shift perturbations (as mentioned above) suggests that the differential line broadening (Fig. 6) observed is predominantly due to a direct interaction with cytP450, enabling the characterization of the interaction interface between cytb$_5$ and cytP450 (63, 64). cytb_5 residues that exhibited significant differential line broadening (with a decrease in peak height of greater than 20% as compared with free cytb$_5$) were mapped onto the NMR structure of cytb$_5$. These residues, which include Glu-48, Glu-49, Asp-65, Val-66, and Thr-70 to Ser-76, highlight a region of cytb$_5$ around the solvent-exposed edge of the heme that potentially forms the interaction interface with cytP450 (Fig. 6*B*). Broadening of His-68 and Ser-69 resonances of cytb$_5$ was also observed and may be due to the close proximity of the paramagnetic center in cytP450 and/or due to steric interaction between His-68 and Ser-69 and residues on cytP450 in the interface. We also observed broadening of the backbone amide-NH resonances corresponding to residues Met-96 to Val-103 in the flexible linker domain of cytb$_5$ (Fig. 5); this observed broadening is likely due to restriction of the motion of the linker upon complex formation (65).

Interestingly, extensive line broadening and disappearance of most of the cytb$_5$ amide resonances in the ^{1}H-^{15}N TROSY-HSQC spectrum were observed upon addition of an equimolar amount of substrate-bound unlabeled cytP450 (Fig. 6*C*). Two different compounds were tested as follows: BHT (type I substrate), and the heme iron-binding inhibitor, 1-(4-chlorophenyl)imidazole (1-CPI; type II ligand).[5] The widespread broadening of the cytb$_5$ resonances might suggest that the interaction of cytb$_5$ with substrate-bound cytP450 has shifted from a fast-to-intermediate (nanosecond to microsecond) to an intermediate-to-slow time scale (microsecond to millisecond), which causes the disappearance of the majority of cytb$_5$ resonances upon titration of substrate-bound cytP450. This conjecture is further supported by the measurement of a submicromolar K_d value for the cytb$_5$-cytP450 complex in the presence of the substrates methoxyflurane ($K_d \sim 0.02$ μM) (Table 3), BHT ($K_d \sim 0.3$ μM) (data not shown), and 1-CPI ($K_d \sim 0.03$ μM) (data not shown) in aqueous solution. These submicromolar K_d values are consistent with an intermediate-to-slow exchange on the NMR time scale leading to extensive line broadening of cytb$_5$ amide resonances (57). A previous kinetic study has also reported a greater than 10-fold decrease in K_d of the cytb$_5$-cytP450 complex upon addition of the substrate, benzphetamine (66). However, due to extensive line broadening and disappearance of most of the resonances of the heme domain of cytb$_5$ in the ^{1}H-^{15}N TROSY-HSQC spectrum, relaxation NMR experiments could not be performed to validate the change in the time scale of interaction.

Mutagenesis Identifies Residues in Contact in the cytb$_5$-cytP450 Complex—To complement the NMR data collected on the cytb$_5$-cytP450 complex, we carried out site-directed mutagenesis of residues on both cytb$_5$ and cytP450 (supplemental Fig. S2*B* and Tables 3 and 4). Residues (Glu-42, Glu-43, Pro-45, Gly-46, Glu-49, Val-50, Glu-53, Gln-54, Asn-62, Asp-65, Val-66, Asp-71, and Leu-75) on the anionic surface surrounding the solvent-exposed heme of cytb$_5$ were mutated to alanine to explore the role of atoms distal to the β-carbon of the wild-type amino acid in binding to cytP4502B4 (supplemental Fig. S2*B*). After purification, the mutant proteins were assayed for their ability to bind cytP4502B4 and stimulate catalysis in an aqueous reconstituted system (Table 3). Of the 13 different single mutations of cytb$_5$, only two, D65A and V66A, exhibited both a significantly lower affinity for cytP4502B4 (15- and 7-fold higher K_d, respectively) and a decreased ability (85 and 43%, respectively) to stimulate cytP4502B4 catalysis (Table 3).

[5] Type I ligands displace the water coordinating the Fe(III) in the heme as the sixth ligand, shifting the Fe(III) spin equilibrium toward the high spin form, whereas type II ligands can replace the water by coordinating to the Fe(III) thereby stabilizing the low spin form.

TABLE 4

Double mutant cycle analysis of mutants of cytP450 and cytb$_5$

A comparison of the difference in free energy of binding values ($\Delta\Delta G$) between mutant and wild-type proteins to determine the residues interacting at the cytb$_5$-cytP450 interface.

cytP450	cytb$_5$	K_d (μM)[a] cytb$_5$-cytP450	Free energy of binding (kcal/mol) ΔG[b] cytb$_5$-cytP450	Difference in free energy of binding (kcal/mol)	
				$\Delta\Delta$[vi]G[v][c][v] of mutant-wild-type	$\Delta\Delta G$[d] interaction of double mutants
Wild type	Wild type	0.022 ± 0.003	−10.43		
R122A	Wild type	0.221 ± 0.010	−9.07	1.36	
Wild type	D65A	0.332 ± 0.032	−8.82	1.61	
R122A	D65A	0.558 ± 0.065	−8.52	1.91	1.06
Wild type	V66A	0.152 ± 0.019	−9.29	1.14	
R122A	V66A	0.814 ± 0.033	−8.29	2.14	0.37
R126A	Wild type	0.454 ± 0.042	−8.64	1.79	
Wild type	D65A	0.332 ± 0.042	−8.82	1.61	
R126A	D65A	18.33 ± 1.500	−6.45	3.98	−0.58
Wild type	V66A	0.152 ± 0.010	−9.29	1.14	
R126A	V66A	5.149 ± 0.930	−7.20	3.23	−0.30
F135A	Wild type	0.205 ± 0.021	−9.11	1.32	
Wild type	D65A	0.332 ± 0.042	−8.82	1.61	
F135A	D65A	1.420 ± 0.110	−7.96	2.47	0.46
Wild type	V66A	0.152 ± 0.010	−9.29	1.14	
F135A	V66A	0.959 ± 0.130	−8.20	2.23	0.23
M137A	Wild type	0.379 ± 0.040	−8.75	1.68	
Wild type	D65A	0.332 ± 0.012	−8.82	1.61	
M137A	D65A	3.951 ± 0.440	−7.36	3.07	0.22
Wild type	V66A	0.152 ± 0.010	−9.29	1.14	
M137A	V66A	1.583 ± 0.142	−7.90	2.53	0.30
K139A	Wild type	0.611 ± 0.050	−8.46	1.97	
Wild type	D65A	0.332 ± 0.012	−8.82	1.61	
K139A	D65A	4.831 ± 0.042	−7.24	3.19	0.38
Wild type	V66A	0.152 ± 0.010	−9.29	1.14	
K139A	V66A	1.683 ± 0.212	−7.86	2.57	0.52
K433A	Wild type	0.458 ± 0.053	−8.63	1.80	
Wild type	D65A	0.332 ± 0.012	−8.82	1.61	
K433A	D65A	0.869 ± 0.071	−8.26	2.17	
Wild type	V66A	0.152 ± 0.010	−9.29	1.14	
K433A	V66A	0.487 ± 0.052	−8.60	1.83	

[a] All K_d values were measured in the presence of methoxyflurane.

[b] Free energy change of binding of the indicated cytP450 and cytb$_5$ is shown.

[c] The difference in free energy of binding between a complex containing a single mutant protein and a complex with two wild-type proteins is shown: $\Delta\Delta G = \Delta G_{\text{mutant}} - \Delta G_{\text{wild type}}$.

[d] The free energy of interaction between the two mutant proteins is shown: $\Delta\Delta G_{\text{interaction of mutants}} = \Delta\Delta G_{\text{mutant cytP450-wild-type cytb5}} + \Delta\Delta G_{\text{wild-type cytP450-mutant cytb5}} - \Delta\Delta G_{\text{mutant cytp450-mutant cytb5}}$.

These data indicate that Asp-65 and Val-66 of cytb$_5$ are important for both binding to cytP450 and its function as an enhancer of cytP450 catalysis. Site-directed mutants of cytb$_5$, P45A, G46A, E53A, Q54A, D71A, and L75A were found to be indistinguishable from wild type (data not shown). Whereas E42A, E43A, E49A, V50A, and N62A exhibited a modest decrease in binding affinity to cytP450, these mutants did not show a decrease in their ability to stimulate cytP4502B4 activity (Table 3); as a result, these residues were deemed to only play a minor role in the interprotein interactions.

Previous mutagenesis studies on cytP4502B4 have shown that residues in the C-helix and C-D loop, which were mutated to alanine (Arg-122, Arg-126, Arg-133, Phe-135, Met-137, and Lys-139) and Lys-433 in the β-bulge near the axial Cys-436, are important for binding to cytb$_5$ (Table 3) (15). The R133A mutant showed a drastic decrease in binding affinity to cytb$_5$; in fact, the binding was too weak to obtain a robust K_d measurement. All other mutants showed a decrease in binding affinity of at least 10-fold.

To determine the amino acids that are in contact at the interface between cytb$_5$ and cytP450, a "double mutant cycle" (15, 67) analysis was then performed using mutants of both cytb$_5$ and cytP450 that are defective in binding to one another (Table 4). In such cycles, the sum of the free energy change for the two single amino acid mutant proteins is compared with that of the double mutant protein complex. When the sum of the free energy change of the single mutants is not equal to that of the double mutant, the two residues are defined as interacting and not behaving independently. This assumes that the two residues are not interacting indirectly, *e.g.* through a structural perturbation (67, 68). A difference of greater than 1.0 kcal/mol was considered significant (67, 68). The free energy of binding, ΔG, of all possible pairs of wild type and poorly binding alanine mutants (Table 3) of both cytP4502B4 (15) (Arg-122, Arg-126, Phe-135, Met-137, Lys-139, and Lys-433) and cytb$_5$ (Asp-65 and Val-66) was measured. Table 4 presents the results of the double mutant cycle analysis, which indicate that Lys-433 of cytP450 interacts with both Asp-65 and Val-66 of cytb$_5$ and that Arg-122 of cytP450 interacts with Asp-65 of cytb$_5$. Because of the 68-fold decreased affinity of the R133A-cytP450 mutant for cytb$_5$, a robust double mutant cycle analysis could not be performed (15); however, R133A-cytP450 mutant's poor affinity for cytb$_5$ indicates that Arg-133 is critical to the interprotein interaction.

Structure of the cytb$_5$-cytP450 Complex—A structural model of the cytb$_5$-cytP450 complex was generated using the data-driven docking program HADDOCK (26), governed by unambiguous and ambiguous intermolecular restraints obtained from mutagenesis and NMR data (Table 5). The solution NMR structure of the heme domain of the membrane-bound rabbit

TABLE 5

List of ambiguous and unambiguous restraints used in HADDOCK

Ambiguous active and passive residues were defined for cytb$_5$ based on differential line broadening and solvent accessibility (>40%) (83). Active and passive residues for cytP450 were defined based on site-directed mutagenesis and solvent accessibility (> 40%) (Ref. Accelrys Software Inc., Discovery Studio Modeling Environment, Release 3.5, San Diego, 2012 Accelrys Software Inc.). Unambiguous restraints were defined based on the double mutant cycle analysis with a lower bound of 2.0 Å.

	cytb$_5$	cytP450
Unambiguous restraints	Asp-65-Arg-122, Val-66-Arg-122,[a] Asp-65-Lys-433, Val-66-Lys4–33	
Ambiguous restraints, Active	Asp-6, Lys-39, Glu-48, Glu-49, Thr-70, Asp-71, Arg-73, Glu-74	Arg-122, Arg-126, Arg-133, Phe-135, Met-137, Lys-139, Lys-433
Ambiguous restraints, Passive	Glu-43, His-44, Pro-45, Gly-46, Glu-47, Val-50, Glu-61, Asn-62, Glu-64, Gl-67, Ser-69, Lys-77	79 residues with >40% solvent accessibility on the proximal side of cytP450 where the heme is closest to the surface

[a] The Arg-122–Val-66 constraint was included in the docking simulations because of the proximity of Val-66 to Asp-65, which is predicted to interact with Arg-122 based on double mutant cycle analysis.

TABLE 6

Energy statistics for the two lowest energy clusters of the complex between cytb$_5$ and cytP450 generated from HADDOCK

Parameters	Cluster I	Cluster II
No. of structures from the 50 lowest energy -docked solutions	21	14
Backbone r.m.s.d. (as compared with the reference structure)	0.81 ± 0.29 Å	2.67 ± 0.42 Å
Total energy	−435.8 ± 38.0 kcal/mol	−470.7 ± 49.7 kcal/mol
van der Waals energy	−43.8 ± 8.0 kcal/mol	−29.5 ± 7.2 kcal/mol
Electrostatic energy	−392.0 ± 37.2 kcal/mol	−441.2 ± 53.7 kcal/mol
Desolvation energy	33.9 ± 3.0 kcal/mol	35.8 ± 3.6 kcal/mol
Interface surface area	937.0 ± 88.0 Å^2	903.1 ± 77.7 Å^2

cytb$_5$ with a backbone r.m.s.d. of 0.32 ± 0.10 Å (Fig. 1*A*) and a 1.9 Å resolution crystal structure of the heme-containing domain of cytP4502B4 (PDB code 1SUO (41)) were used in HADDOCK calculations. Docking was performed in the absence of a membrane environment, and therefore our structure of the complex reveals the interactions between the structured heme domains of cytb$_5$ and cytP450. However, it is important to note that all NMR and mutagenesis data were collected on membrane-bound full-length proteins, and the enzymatic function of the complex under these conditions was confirmed by activity assays (supplemental Table S1).

As described above, the double mutant cycle analysis revealed that Lys-433 of cytP450 interacts with both Asp-65 and Val-66 of cytb$_5$ and that Arg-122 of cytP450 interacts with Asp-65 of cytb$_5$; these interactions were incorporated as unambiguous intermolecular restraints in HADDOCK. The ambiguous intermolecular restraints were generated using active and passive residues for cytb$_5$ and cytP450 (all >40% solvent-accessible). As active residues, eight cytb$_5$ residues exhibiting significant differential line broadening upon complex formation with cytP450, and seven cytP450 residues deemed essential for binding to cytb$_5$, based on site-directed mutagenesis, were selected. As passive residues, solvent-accessible (>40% solvent-accessible) amino acids flanking the active residues were selected for cytb$_5$, and for cytP450, all residues on the proximal side where the heme is closest to the surface were selected (Table 5).

The docking simulations reveal not a single specific complex but rather an ensemble of low energy complex orientations (supplemental Fig. S3*A*), where the acidic convex surface of cytb$_5$ is sampling an extended surface area on the concave basic proximal side of cytP450 (data not shown). The two dominant subpopulations of low energy complexes (Table 6 and supplemental Fig. S3), titled clusters I and II, include two unique but overlapping clusters of residues on cytb$_5$ and cytP4502B4 (Figs. 7 and 8, supplemental Figs S2 and S3, and supplemental Table S2). The residues of cytb$_5$ that are common between the majority of the low energy complex structures (supplemental Fig. S3) are found mostly on the α4 and α5 helices). The cytP450 and cytb$_5$ hemes are nearly perpendicular to one another in both clusters, and the shortest distance between the two heme edges is 9.0 and 7.4 Å, respectively, in clusters I and II, which is well within the 14.0 Å limit predicted for efficient electron transfer (Fig. 7*B*) (69). The Fe-Fe distance is 20.9 and 19.3 Å in clusters I and II, respectively.

DISCUSSION

The structure of the heme domain of full-length rabbit cytb$_5$, incorporated in DPC micelles, was found to be similar but not identical to the previously reported structure of truncated rabbit cytb$_5$ (18). Our NMR structure has additional β-strands (β1 and β4) and longer (α1, β2, α2, and α3) and shorter (β5 and 3_{10} helix) segments for some of the secondary structure elements (Figs. 1 and 3 and supplemental Fig. S1*A*). The linker region (Ser-90 to Asp-104) in our NMR structure of cytb$_5$, which connects the cytosolic heme domain to the α-helical transmembrane anchor, was found to be random coil. As mentioned under "Results," the extended form of the cytb$_5$ linker region likely allows for proper interaction of the cytb$_5$ soluble domain with its redox partners. Solid-state SLF NMR data, in combination with a structure fitting algorithm (54), were used to determine the α-helical structure of the transmembrane domain of cytb$_5$ (Fig. 1*C*). Our NMR structure of full-length microsomal ferric cytb$_5$ was used subsequently to establish the interaction interface between microsomal, rabbit, ferric cytb$_5$, and cytP450.

cytb$_5$-cytP450 Interaction Interface—As mentioned above, the modest average chemical shift perturbations ($\Delta\delta$ <0.01 ppm) observed for the heme domain of full-length cytb$_5$ upon complex formation with substrate-free cytP450 could be a result of the combination of interaction on the fast-to-interme-

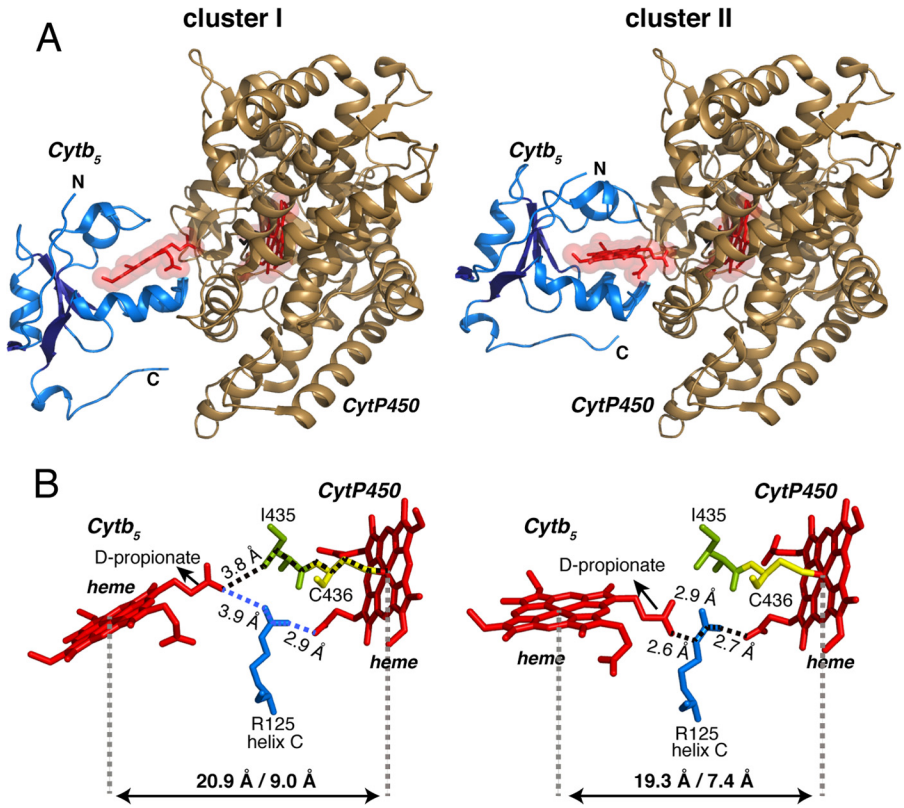

FIGURE 7. **Structure of the full-length membrane-bound cytb$_5$-cytP450 complex.** *A,* two lowest energy clusters (*I* and *II*) of the complex between the catalytic heme-binding domains of rabbit cytb$_5$ (NMR structure; *blue*) and cytP4502B4 (PDB code 1SUO (41); in *gold*) generated from HADDOCK, driven by NMR, and mutagenesis restraints. Heme molecules are presented in *red. B,* proposed electron transfer pathway between the redox centers of cytb$_5$ and cytP450 are presented as *broken lines*. The shortest electron transfer pathway predicted using HARLEM (76) is shown in the *black dotted lines* for clusters I and II. The shortest heme-edge to heme-edge distance is 7.4 and 9.0 Å in clusters II and I, respectively.

diate NMR exchange time scale and formation of an ensemble of dynamic encounter complexes, as has been reported previously for other metalloprotein complexes (59, 62). Complex formation between electron transfer proteins, like cytP450 and cytb$_5$, has been shown to proceed via the formation of dynamic encounter complexes driven by the oppositely charged surfaces of the proteins (supplemental Fig. S2*A*) (62, 70). In our experiment, we hypothesize that the different complex orientations, within the encounter complexes, are interchanging among themselves at a fast-to-intermediate time scale, because we do not see any significant chemical shift perturbations. These encounter complexes formed by cytb$_5$ and cytP450 in the absence of a substrate are most likely in equilibrium with a well defined complex orientation, known as the stereospecific complex (70). The stereospecific complex is characterized by a tighter affinity of the two proteins for one another and more hydrophobic interactions, whereas the weaker encounter complexes are stabilized predominantly by long range electrostatic interactions. The lifetime and the populations of the individual orientations govern the effect of the encounter and the stereospecific complex on the NMR data.

The extensive line broadening of cytb$_5$ resonances upon complex formation with substrate-bound cytP450 (Fig. 6) suggests that substrate binding modulates the affinity of the proteins for each other. Our result is in agreement with two recent studies where binding of the substrate modulates the interaction between cytP450 and cytb$_5$ (58, 65). Addition of the substrate could be shifting the equilibrium from the weaker encounter complexes toward the stereospecific complex.

The two lowest energy cytb$_5$-cytP450 complex orientations (clusters I and II), calculated from HADDOCK driven by the NMR and mutagenesis data presented here, likely represent "productive" cytb$_5$-cytP450 complex orientations, because the heme-edge to heme-edge distances would allow for efficient electron transfer (69). Both complex structures are typical of other redox complexes in that, although there is a large interfacial area of contact (~937 Å^2 in cluster I and ~903 Å^2 in cluster II, see Table 6), the bulk of the binding energy can be attributed to a small number of complementary residues (71). Our result is in agreement with a recent chemical cross-linking study on cytP4502B4 where the authors observed evidence for the existence of two mutual orientations of the cytb$_5$-cytP450 complex (72).

The cytb$_5$-cytP450 complex orientations reveal that the acidic convex surface of cytb$_5$ docks, like a ball in a socket, into the entire concavity on the proximal surface of cytP450, with the C-helix residues contributing the vast majority of the binding energy as indicated by the mutagenesis data (Table 3). A closer look at the complex structures from clusters I and II (Fig. 8, supplemental Fig. S2, *C* and *D*, and supplemental Table S2) highlights that the interactions at the complex interface occur between 14 residues and the heme-D-propionate of cytb$_5$ and 14 residues of cytP450. Based on the double mutant cycle analysis (Table 4), we identified that the interactions contributing

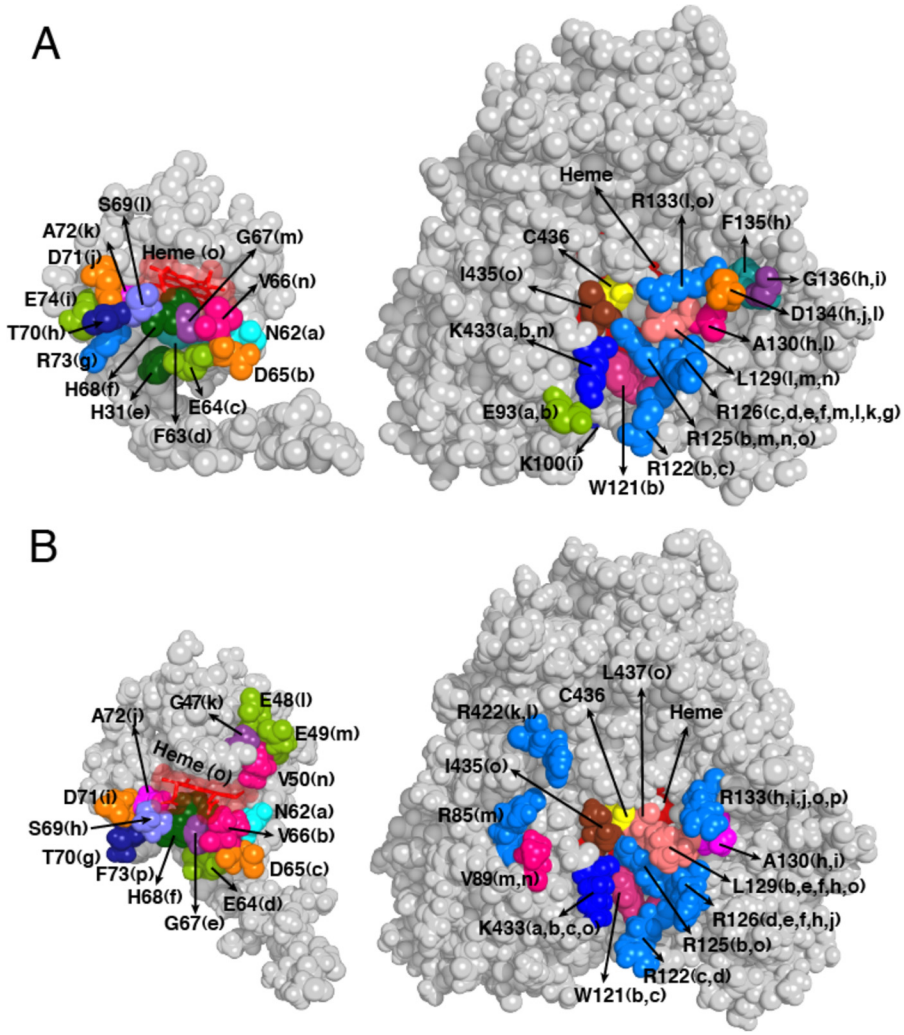

FIGURE 8. **Binding interface of the membrane-bound cytb$_5$-cytP450 complex.** The complex is presented by opening the complex-like pages of a book with the interaction interface of cytb$_5$ and cytP450 facing the viewer. The space-filling model of cytb$_5$ (NMR structure) and cytP450 (PDB code 1SUO (41)) is presented highlighting the interfacial residues involved in protein-protein contacts in cluster I (*A*) and cluster II (*B*) complex structures. Residues on cytb$_5$ that are in contact with residues on cytP450 are denoted with matching letters in *parentheses*. For example, Asp-65 (*orange*) on cytb$_5$ is H-bonding to Arg-122 (*blue*) on cytP450 in *A*. Arg-125 highlighted in *blue* is H-bonded to the heme-D-propionate in *B*. An important point to note is that the residues on cytb$_5$ and cytP450, which form the interaction interface, are largely the same between the two clusters and are mostly present on the lower edge (residues on α4 and α5 helix) of the soluble domain surrounding the heme. The residues in the interface are in excellent agreement with our NMR data and site-directed mutagenesis presented here (Tables 3 and 4), as well as elsewhere (15).

the most binding energy to the complex formation were between the cytP450 C-helix residue Arg-122 and Lys-433 in the β-bulge (near the axial Cys-436) and Asp-65 and Val-66 at the C terminus of helix α4 of cytb$_5$. These interactions were shown to be critical for both complex formation and function. From the HADDOCK structures, we see that Asp-65 of cytb$_5$ is able to form hydrogen bonds and/or salt bridges with Arg-122 and Lys-433 of cytP450 and that Val-66 of cytb$_5$ is in van der Waals contact with Lys-433 (and Arg-125) of cytP450. Arg-133 of cytP450, which was found to be very important for binding to cytb$_5$ in our studies, is hydrogen-bonded with the heme propionate group on cytb$_5$ in both clusters (additional interactions were also found for Arg-133 in cluster II, see supplemental Table S2). The function of other cytP4502B4 residues previously mutated to alanine (Table 3) (15) can also be discussed. Arg-126 of cytP450 was found to form hydrogen bonds and salt bridges with Glu-64 of cytb$_5$ in both clusters and hydrogen bonds with His-68 (supplemental Table S2). Surprisingly, the C-D loop residues of cytP450, Met-137, and Lys-139, which mutagenesis data revealed were important for cytb$_5$ binding (Table 3), were not in the complex interface (Fig. 8 and supplemental Fig. S2, *C* and *D*). We hypothesize that their mutation might induce a structural perturbation in the flexible C-helix, which in turn destabilizes the interaction with cytb$_5$. The K139A mutation was previously shown to disrupt a hydrogen bond network between the Lys-139 amino group and Pro-261 and Asn-260 in the G-H loop (41), suggesting an allosteric interaction between the C-helix and the G-H loop. Arg-422 on cytP450, which is in contact with cytb$_5$ in the predicted complex structure from cluster II, was previously considered to be important only for binding to CPR (15). However, review of the previously reported mutagenesis data revealed that the R422A-cytP450 mutant exhibited a 50% decreased affinity for cytb$_5$, which at the time was considered insignificant (15). Residue Arg-443, which was shown to be important only for cytP450 reductase (15), is not found in the interaction interface of the predicted complex structures (Fig. 8).

On cytb$_5$, both Asp-65 and Val-66, which were shown to be in the binding site for cytochrome *c* (18, 73), are now shown to be in the binding site for cytP4502B4 both experimentally and in our HADDOCK complex structures. A double cytb$_5$ mutant E48G and E49G mutant (which introduced a very flexible sequence of four glycine residues) has been shown to be deficient in its ability to stimulate the activity of cytP450c17 (74). This observation is consistent with the presence of Glu-48 and Glu-49 in the interaction interface of cluster II and is in accordance with our NMR data where we observed considerable line broadening for Glu-48 and Glu-49 upon complex formation with cytP450.

The HADDOCK structures of the cytb$_5$-cytP450 complex, as well as previous experiments (7, 14), demonstrate that cytb$_5$ and CPR compete for an overlapping binding site on cytP450, and they rule out the existence of separate functional binding sites for cytb$_5$ and CPR and the formation of a ternary complex between the three proteins (75).

Electron Transfer Pathway between cytb$_5$ and cytP450—The structure of the cytb$_5$-cytP450 complex generated from HADDOCK shows that the guanidinium group of Arg-125 on the C-helix of cytP450 forms a salt bridge between the heme-D-propionates of both cytb$_5$ and cytP450. This network was predicted, using HARLEM (76), to serve as one of the shortest electron transfer pathways between the two proteins (Fig. 7*B*). Arg-125 is one of the most highly conserved cytP450 residues. It is homologous to Arg-112 in cytP450$_{cam}$, which has been shown to be essential for electron transfer (77). The physiological significance of Arg-125 was also highlighted when mutation of the Arg-125 homolog in human cytP45024A1 resulted in a defect in vitamin D degradation (78). We have previously attempted to characterize the R125A mutant of cytP4502B4 (15), and we found that the mutation rendered the protein unstable. The proposed network involving the heme propionates is consistent with previous studies that have demonstrated that the heme propionate groups of cytb$_5$ interact with charged groups on cytochrome *c* (79, 80) and cytP450 isozymes (81), suggesting that other cytP450 complexes employ a similar interface. Fig. 7*B* presents another possible electron transfer pathway between the heme-D-propionate of cytb$_5$ and Ile-435, the nonconserved amino acid preceding the axial ligand, Cys-436, on cytP450. However, our mutagenesis data have shown that the I435A mutant is as active as the wild-type cytP450 (data not shown), suggesting that it does not play a critical role in electron transfer between the two proteins.

Conclusion—Here, we have presented the first full-length structure of rabbit cytb$_5$ incorporated in a membrane mimetic (DPC micelles or lipid bicelles) obtained using a combination of solution and solid-state NMR spectroscopy. The heme domain and linker region structures were established using solution NMR, and the transmembrane domain structure and topology were identified using solid-state NMR (full-length cytb$_5$ was used for all NMR measurements). The highly conserved nature of the transmembrane domain of cytb$_5$ (with a sequence similarity of 78–96% (23) among vertebrates) suggests that these results and methodology should be applicable to other mammalian cytsb$_5$ as well.

Subsequently, HADDOCK (26), driven by experimental constraints obtained from site-directed mutagenesis and solution NMR spectroscopy on full-length membrane-bound microsomal cytb$_5$ and cytP4502B4, was used to generate a model of the cytb$_5$-cytP450 complex. The two proteins form a dynamic complex mediated by both hydrophobic and electrostatic interactions (Fig. 8 and supplemental Table S2). The electrostatic interactions between the oppositely charged residues, as well as the fact that the two proteins are anchored in the membrane, play important roles in orienting the two proteins prior to complex formation and help considerably by increasing the number of productive collisions that control and direct the flow of electrons from cytb$_5$ to cytP450. Addition of a small molecule substrate (BHT) or inhibitor (1-CPI) significantly increased the binding affinity between cytb$_5$ and cytP450, moving the dynamic interaction between the two proteins from a fast-to-intermediate regime to an intermediate-to-slow regime on the NMR time scale, based on the extensive line broadening of cytb$_5$ amide NMR resonances upon complex formation with substrate-bound cytP450. The structure of the cytb$_5$-cytP450 complex presented allows us to identify the interactions at the interface and to propose the pathway of interprotein electron transfer from cytb$_5$ to cytP450 through the highly conserved Arg-125 residue on cytP450. Our study demonstrates how a combinatorial approach, involving NMR and mutagenesis studies, can be exploited to obtain atomic level structural, functional, and dynamic information on intact, membrane-bound, and large metalloprotein redox complexes in a near-native environment. The extensive knowledge of the structure of the cytb$_5$-cytP450 complex provides insights into the principles governing interprotein interactions and will markedly facilitate our ability to unravel the molecular mechanism by which the rate of cytP450 catalysis is regulated by its redox partners, cytb$_5$ and CPR.

REFERENCES

1. Guengerich, F. P., Wu, Z. L., and Bartleson, C. J. (2005) Function of human cytochrome P450s: characterization of the orphans. *Biochem. Biophys. Res. Commun.* **338,** 465–469
2. Shen, A. L., O'Leary, K. A., and Kasper, C. B. (2002) Association of multiple developmental defects and embryonic lethality with loss of microsomal NADPH-cytochrome p450 oxidoreductase. *J. Biol. Chem.* **277,** 6536–6541
3. Nebert, D. W., and Russell, D. W. (2002) Clinical importance of the cytochromes P450. *Lancet* **360,** 1155–1162
4. O'Donnell, A., Judson, I., Dowsett, M., Raynaud, F., Dearnaley, D., Mason, M., Harland, S., Robbins, A., Halbert, G., Nutley, B., and Jarman, M. (2004) Hormonal impact of the 17α-hydroxylase/C(17,20)-lyase inhibitor abiraterone acetate (CB7630) in patients with prostate cancer. *Br. J. Cancer* **90,** 2317–2325
5. Orlando, L., Schiavone, P., Fedele, P., Calvani, N., Nacci, A., Rizzo, P., Marino, A., D'Amico, M., Sponziello, F., Mazzoni, E., Cinefra, M., Fazio, N., Maiello, E., Silvestris, N., Colucci, G., and Cinieri, S. (2010) Molecularly targeted endocrine therapies for breast cancer. *Cancer Treat. Rev.* **36,** S67–S71
6. Im, S. C., and Waskell, L. (2011) The interaction of microsomal cytochrome P450 2B4 with its redox partners, cytochrome P450 reductase, and cytochrome b_5. *Arch. Biochem. Biophys.* **507,** 144–153
7. Zhang, H., Hamdane, D., Im, S. C., and Waskell, L. (2008) Cytochrome b_5 inhibits electron transfer from NADPH-cytochrome P450 reductase to ferric cytochrome P450 2B4. *J. Biol. Chem.* **283,** 5217–5225
8. Gruenke, L. D., Konopka, K., Cadieu, M., and Waskell, L. (1995) The stoichiometry of the cytochrome P-450-catalyzed metabolism of me-

thoxyflurane and benzphetamine in the presence and absence of cytochrome b_5. *J. Biol. Chem.* **270,** 24707–24718
9. Finn, R. D., McLaughlin, L. A., Ronseaux, S., Rosewell, I., Houston, J. B., Henderson, C. J., and Wolf, C. R. (2008) Defining the *in vivo* role for cytochrome b_5 in cytochrome P450 function through the conditional hepatic deletion of microsomal cytochrome b_5. *J. Biol. Chem.* **283,** 31385–31393
10. Guengerich, F. P. (2006) Cytochrome P450s and other enzymes in drug metabolism and toxicity. *AAPS J.* **8,** E101–E111
11. Shimada, T., Mernaugh, R. L., and Guengerich, F. P. (2005) Interactions of mammalian cytochrome P450, NADPH-cytochrome P450 reductase, and cytochrome b_5 enzymes. *Arch. Biochem. Biophys.* **435,** 207–216
12. Canova-Davis, E., Chiang, J. Y., and Waskell, L. (1985) Obligatory role of cytochrome b_5 in the microsomal metabolism of methoxyflurane. *Biochem. Pharmacol.* **34,** 1907–1912
13. Morgan, E. T., and Coon, M. J. (1984) Effects of cytochrome b_5 on cytochrome P-450-catalyzed reactions. Studies with manganese-substituted cytochrome b_5. *Drug Metab. Dispos.* **12,** 358–364
14. Zhang, H., Im, S. C., and Waskell, L. (2007) Cytochrome b_5 increases the rate of product formation by cytochrome P450 2B4 and competes with cytochrome P450 reductase for a binding site on cytochrome P450 2B4. *J. Biol. Chem.* **282,** 29766–29776
15. Bridges, A., Gruenke, L., Chang, Y. T., Vakser, I. A., Loew, G., and Waskell, L. (1998) Identification of the binding site on cytochrome P450 2B4 for cytochrome b_5 and cytochrome P450 reductase. *J. Biol. Chem.* **273,** 17036–17049
16. Halpert, J. R. (2011) Structure and function of cytochromes P450 2B: from mechanism-based inactivators to x-ray crystal structures and back. *Drug Metab. Dispos.* **39,** 1113–1121
17. Scott, E. E., He, Y. A., Wester, M. R., White, M. A., Chin, C. C., Halpert, J. R., Johnson, E. F., and Stout, C. D. (2003) An open conformation of mammalian cytochrome P450 2B4 at 1.6-Å resolution. *Proc. Natl. Acad. Sci. U.S.A.* **100,** 13196–13201
18. Banci, L., Bertini, I., Rosato, A., and Scacchieri, S. (2000) Solution structure of oxidized microsomal rabbit cytochrome b_5. Factors determining the heterogeneous binding of the heme. *Eur. J. Biochem.* **267,** 755–766
19. Nunez, M., Guittet, E., Pompon, D., van Heijenoort, C., and Truan, G. (2010) NMR structure note: oxidized microsomal human cytochrome b_5. *J. Biomol. NMR* **47,** 289–295
20. Başaran, N., Doebler, R. W., Goldston, H., and Holloway, P. W. (1999) Effect of lipid unsaturation on the binding of native and a mutant form of cytochrome b_5 to membranes. *Biochemistry* **38,** 15245–15252
21. Greenhut, S. F., Taylor, K. M., and Roseman, M. A. (1993) Tight insertion of cytochrome b_5 into large unilamellar vesicles. *Biochim. Biophys. Acta* **1149,** 1–9
22. Chester, D. W., Skita, V., Young, H. S., Mavromoustakos, T., and Strittmatter, P. (1992) Bilayer structure and physical dynamics of the cytochrome b_5 dimyristoylphosphatidylcholine interaction. *Biophys. J.* **61,** 1224–1243
23. Clarke, T. A., Im, S. C., Bidwai, A., and Waskell, L. (2004) The role of the length and sequence of the linker domain of cytochrome b_5 in stimulating cytochrome P450 2B4 catalysis. *J. Biol. Chem.* **279,** 36809–36818
24. Chudaev, M. V., Gilep, A. A., and Usanov, S. A. (2001) Site-directed mutagenesis of cytochrome b_5 for studies of its interaction with cytochrome P450. *Biochemistry* **66,** 667–681
25. Vergéres, G., and Waskell, L. (1995) Cytochrome b_5, its functions, structure, and membrane topology. *Biochimie* **77,** 604–620
26. de Vries, S. J., van Dijk, A. D., Krzeminski, M., van Dijk, M., Thureau, A., Hsu, V., Wassenaar, T., and Bonvin, A. M. (2007) HADDOCK *versus* HADDOCK: new features and performance of HADDOCK2.0 on the CAPRI targets. *Proteins* **69,** 726–733
27. Saribas, A. S., Gruenke, L., and Waskell, L. (2001) Overexpression and purification of the membrane-bound cytochrome P450 2B4. *Protein Expr. Purif.* **21,** 303–309
28. Mulrooney, S. B., and Waskell, L. (2000) High level expression in *Escherichia coli* and purification of the membrane-bound form of cytochrome b_5. *Protein Expr. Purif.* **19,** 173–178
29. Dürr, U. H., Yamamoto, K., Im, S. C., Waskell, L., and Ramamoorthy, A. (2007) Solid-state NMR reveals structural and dynamical properties of a membrane-anchored electron-carrier protein, cytochrome b_5. *J. Am. Chem. Soc.* **129,** 6670–6671
30. Omura, T., and Sato, R. (1967) Isolation of cytochromes P-450 and P-420. *Methods Enzymol.* **10,** 556–561
31. Harris, R. K., Becker, E. D., Cabral de Menezes, S. M., Goodfellow, R., and Granger, P. (2002) NMR nomenclature: Nuclear spin properties and conventions for chemical shifts. IUPAC recommendations 2001. *Solid State Nucl. Magn. Reson.* **22,** 458–483
32. Delaglio, F., Grzesiek, S., Vuister, G. W., Zhu, G., Pfeifer, J., and Bax, A. (1995) NMRPipe: a multidimensional spectral processing system based on UNIX pipes. *J. Biomol. NMR* **6,** 277–293
33. Kneller, D. G., and Kuntz, I. D. (1993) UCSF Sparky-an NMR display, annotation, and assignment tool. *J. Cell. Biochem.* **53,** 254–254
34. Cornilescu, G., Delaglio, F., and Bax, A. (1999) Protein backbone angle restraints from searching a database for chemical shift and sequence homology. *J. Biomol. NMR* **13,** 289–302
35. Güntert, P., Mumenthaler, C., and Wüthrich, K. (1997) Torsion angle dynamics for NMR structure calculation with the new program DYANA. *J. Mol. Biol.* **273,** 283–298
36. Güntert, P. (2004) Automated NMR structure calculation with CYANA. *Methods Mol. Biol.* **278,** 353–378
37. Dvinskikh, S. V., Yamamoto, K., and Ramamoorthy, A. (2006) Heteronuclear isotropic mixing separated local field NMR spectroscopy. *J. Chem. Phys.* **125,** 34507
38. Caravatti, P., Braunschweiler, L., and Ernst, R. R. (1983) Heteronuclear correlation spectroscopy in rotating solids. *Chem. Phys. Lett.* **100,** 305–310
39. Fung, B. M., Khitrin, A. K., and Ermolaev, K. (2000) An improved broadband decoupling sequence for liquid crystals and solids. *J. Magn. Reson.* **142,** 97–101
40. Dominguez, C., Boelens, R., and Bonvin, A. M. (2003) HADDOCK: a protein-protein docking approach based on biochemical or biophysical information. *J. Am. Chem. Soc.* **125,** 1731–1737
41. Scott, E. E., White, M. A., He, Y. A., Johnson, E. F., Stout, C. D., and Halpert, J. R. (2004) Structure of mammalian cytochrome P450 2B4 complexed with 4-(4-chlorophenyl)imidazole at 1.9-Å resolution: insight into the range of P450 conformations and the coordination of redox partner binding. *J. Biol. Chem.* **279,** 27294–27301
42. Schüttelkopf, A. W., and van Aalten, D. M. (2004) PRODRG: a tool for high throughput crystallography of protein-ligand complexes. *Acta Crystallogr. D Biol. Crystallogr.* **60,** 1355–1363
43. Krissinel, E., and Henrick, K. (2007) Inference of macromolecular assemblies from crystalline state. *J. Mol. Biol.* **372,** 774–797
44. Potterton, E., Briggs, P., Turkenburg, M., and Dodson, E. (2003) A graphical user interface to the CCP4 program suite. *Acta Crystallogr. D Biol. Crystallogr.* **59,** 1131–1137
45. Zhang, Q., Cao, C., Wang, Z. Q., Wang, Y. H., Wu, H., and Huang, Z. X. (2004) The comparative study on the solution structures of the oxidized bovine microsomal cytochrome b_5 and mutant V45H. *Protein Sci.* **13,** 2161–2169
46. Lee, K. B., La Mar, G. N., Kehres, L. A., Fujinari, E. M., Smith, K. M., Pochapsky, T. C., and Sligar, S. G. (1990) ^{1}H NMR study of the influence of hydrophobic contacts on protein-prosthetic group recognition in bovine and rat ferricytochrome b_5. *Biochemistry* **29,** 9623–9631
47. Nguyen, K. T., Soong, R., Lm, S. C., Waskell, L., Ramamoorthy, A., and Chen, Z. (2010) Probing the spontaneous membrane insertion of a tail-anchored membrane protein by sum frequency generation spectroscopy. *J. Am. Chem. Soc.* **132,** 15112–15115
48. Sanders, C. R., Hare, B. J., Howard, K. P., and Prestegard, J. H. (1994) Magnetically oriented phospholipid micelles as a tool for the study of membrane-associated molecules. *Prog. Nucl. Magn. Reson. Spectrosc.* **26,** 421–444
49. Dürr, U. H., Gildenberg, M., and Ramamoorthy, A. (2012) The magic of bicelles lights up membrane protein structure. *Chem. Rev.* **112,** 6054–6074
50. Soong, R., Smith, P. E., Xu, J., Yamamoto, K., Im, S. C., Waskell, L., and Ramamoorthy, A. (2010) Proton-evolved local-field solid-state NMR

studies of cytochrome b_5 embedded in bicelles, revealing both structural and dynamical information. *J. Am. Chem. Soc.* **132,** 5779–5788
51. Dailey, H. A., and Strittmatter, P. (1978) Structural and functional properties of membrane binding segment of cytochrome b_5. *J. Biol. Chem.* **253,** 8203–8209
52. Holloway, P. W., and Buchheit, C. (1990) Topography of the membrane-binding domain of cytochrome-B5 in lipids by Fourier-transform infrared-spectroscopy. *Biochemistry* **29,** 9631–9637
53. Denny, J. K., Wang, J., Cross, T. A., and Quine, J. R. (2001) PISEMA powder patterns and PISA wheels. *J. Magn. Reson.* **152,** 217–226
54. Nevzorov, A. A., and Opella, S. J. (2003) Structural fitting of PISEMA spectra of aligned proteins. *J. Magn. Reson.* **160,** 33–39
55. Vergères, G., and Waskell, L. (1992) Expression of cytochrome b_5 in yeast and characterization of mutants of the membrane-anchoring domain. *J. Biol. Chem.* **267,** 12583–12591
56. Prudêncio, M., and Ubbink, M. (2004) Transient complexes of redox proteins: structural and dynamic details from NMR studies. *J. Mol. Recognit.* **17,** 524–539
57. Zuiderweg, E. R. (2002) Mapping protein-protein interactions in solution by NMR spectroscopy. *Biochemistry* **41,** 1–7
58. Estrada, D. F., Laurence, J. S., and Scott, E. E. (2013) Substrate-modulated cytochrome P450 17A1 and cytochrome b_5 interactions revealed by NMR. *J. Biol. Chem.* **288,** 17008–17018
59. Volkov, A. N., Ferrari, D., Worrall, J. A., Bonvin, A. M., and Ubbink, M. (2005) The orientations of cytochrome *c* in the highly dynamic complex with cytochrome b_5 visualized by NMR and docking using HADDOCK. *Protein Sci.* **14,** 799–811
60. Tang, C., Iwahara, J., and Clore, G. M. (2006) Visualization of transient encounter complexes in protein-protein association. *Nature* **444,** 383–386
61. Volkov, A. N., Ubbink, M., and van Nuland, N. A. (2010) Mapping the encounter state of a transient protein complex by PRE NMR spectroscopy. *J. Biomol. NMR* **48,** 225–236
62. Suh, J. Y., Tang, C., and Clore, G. M. (2007) Role of electrostatic interactions in transient encounter complexes in protein-protein association investigated by paramagnetic relaxation enhancement. *J. Am. Chem. Soc.* **129,** 12954–12955
63. Matsuo, H., Walters, K. J., Teruya, K., Tanaka, T., Gassner, G. T., Lippard, S. J., Kyogoku, Y., and Wagner, G. (1999) Identification by NMR spectroscopy of residues at contact surfaces in large, slowly exchanging macromolecular complexes. *J. Am. Chem. Soc.* **121,** 9903–9904
64. Zamoon, J., Nitu, F., Karim, C., Thomas, D. D., and Veglia, G. (2005) Mapping the interaction surface of a membrane protein: unveiling the conformational switch of phospholamban in calcium pump regulation. *Proc. Natl. Acad. Sci. U.S.A.* **102,** 4747–4752
65. Koberova, M., Jecmen, T., Sulc, M., Cerna, V., Kizek, R., Stiborova, M., and Hodek, P. (2013) Photo-cytochrome b_5–a new tool to study the cytochrome P450 electron-transport chain. *Int. J. Electrochem. Sci.* **8,** 125–134
66. Tamburini, P. P., and Gibson, G. G. (1983) Thermodynamic studies of the protein-protein interactions between cytochrome P-450 and cytochrome b_5. Evidence for a central role of the cytochrome P-450 spin state in the coupling of substrate and cytochrome b_5 binding to the terminal hemoprotein. *J. Biol. Chem.* **258,** 13444–13452
67. Frisch, C., Schreiber, G., Johnson, C. M., and Fersht, A. R. (1997) Thermodynamics of the interaction of barnase and barstar: changes in free energy *versus* changes in enthalpy on mutation. *J. Mol. Biol.* **267,** 696–706
68. Harel, M., Cohen, M., and Schreiber, G. (2007) On the dynamic nature of the transition state for protein-protein association as determined by double-mutant cycle analysis and simulation. *J. Mol. Biol.* **371,** 180–196
69. Page, C. C., Moser, C. C., and Dutton, P. L. (2003) Mechanism for electron transfer within and between proteins. *Curr. Opin. Chem. Biol.* **7,** 551–556
70. Ubbink, M. (2009) The courtship of proteins: Understanding the encounter complex. *FEBS Lett.* **583,** 1060–1066
71. Clackson, T., and Wells, J. A. (1995) A hot spot of binding energy in a hormone-receptor interface. *Science* **267,** 383–386
72. Sulc, M., Jecmen, T., Snajdrova, R., Novak, P., Martinek, V., Hodek, P., Stiborova, M., and Hudecek, J. (2012) Mapping of interaction between cytochrome P450 2B4 and cytochrome b_5: the first evidence of two mutual orientations. *Neuro Endocrinol. Lett.* **33,** 41–47
73. Shao, W., Im, S. C., Zuiderweg, E. R., and Waskell, L. (2003) Mapping the binding interface of the cytochrome b_5-cytochrome *c* complex by nuclear magnetic resonance. *Biochemistry* **42,** 14774–14784
74. Naffin-Olivos, J. L., and Auchus, R. J. (2006) Human cytochrome b_5 requires residues E48 and E49 to stimulate the 17,20-lyase activity of cytochrome P450c17. *Biochemistry* **45,** 755–762
75. Tamburini, P. P., and Schenkman, J. B. (1987) Purification to homogeneity and enzymological characterization of a functional covalent complex composed of cytochromes P-450 isozyme 2 and b_5 from rabbit liver. *Proc. Natl. Acad. Sci. U.S.A.* **84,** 11–15
76. Kurnikov, I. V. (2000) *HARLEM Molecular Modeling Package,* Version 1.0, Department of Chemistry, University of Pittsburgh, Pittsburgh
77. Nakamura, K., Horiuchi, T., Yasukochi, T., Sekimizu, K., Hara, T., and Sagara, Y. (1994) Significant contribution of arginine 112 and its positive charge of *Pseudomonas putida* cytochrome P-450cam in the electron transport from putidaredoxin. *Biochim. Biophys. Acta* **1207,** 40–48
78. Schlingmann, K. P., Kaufmann, M., Weber, S., Irwin, A., Goos, C., John, U., Misselwitz, J., Klaus, G., Kuwertz-Bröking, E., Fehrenbach, H., Wingen, A. M., Güran, T., Hoenderop, J. G., Bindels, R. J., Prosser, D. E., Jones, G., and Konrad, M. (2011) Mutations in CYP24A1 and idiopathic infantile hypercalcemia. *N. Engl. J. Med.* **365,** 410–421
79. Rodgers, K. K., Pochapsky, T. C., and Sligar, S. G. (1988) Probing the mechanisms of macromolecular recognition-the cytochrome-b_5-cytochrome *c* complex. *Science* **240,** 1657–1659
80. Deep, S., Im, S. C., Zuiderweg, E. R., and Waskell, L. (2005) Characterization and calculation of a cytochrome *c*-cytochrome b_5 complex using NMR data. *Biochemistry* **44,** 10654–10668
81. Tamburini, P. P., and Schenkman, J. B. (1986) Mechanism of interaction between cytochromes P-450 RLM5 and b_5: evidence for an electrostatic mechanism involving cytochrome b_5 heme propionate groups. *Arch. Biochem. Biophys.* **245,** 512–522
82. Popovych, N., Sun, S., Ebright, R. H., and Kalodimos, C. G. (2006) Dynamically driven protein allostery. *Nat. Struct. Mol. Biol.* **13,** 831–838
83. Ahmad, S., Gromiha, M., Fawareh, H., and Sarai, A. (2004) ASAView: database and tool for solvent accessibility representation in proteins. *BMC Bioinformatics* **5,** 51